Ecole Centrale de Nantes (ECN)
Institut de Recherche en Génie Civil et Méchanique (GeM)
The International Center for Numerical Methods in Engineering
(CIMNE)

Master of Science Thesis

Numerical Analysis of Cohesive Crack Growth Using Extended Finite Element Method (X-FEM)

by

Saeid Mojiri

Supervisor: Nicolas Chevaugeon

Nantes, France, 2010

To my wife Parisa

Contents

Contents i

1 Introduction 3

2 Fracture mechanics and cohesive crack model 7
- 2.1 Fracture mechanics . . . 7
  - 2.1.1 Linear Elastic vs Elastic Plastic Fracture Mechanics . . . 7
  - 2.1.2 Loading modes . . . 8
  - 2.1.3 Process region . . . 8
  - 2.1.4 Energy release rate . . . 9
  - 2.1.5 Stress intensity factor . . . 9
  - 2.1.6 J-integral . . . 10
  - 2.1.7 Strain softening and snap back phenomenon . . . 11
  - 2.1.8 Size effects . . . 12
- 2.2 Cohesive crack model . . . 15
  - 2.2.1 Modeling of fracture process region . . . 15
  - 2.2.2 Basic concepts of cohesive crack model . . . 16
  - 2.2.3 Crack propagation criterion . . . 17
  - 2.2.4 Size effects in cohesive crack model . . . 17
  - 2.2.5 Brittleness number . . . 18

3 Numerical methods 19
- 3.1 Finite Element Method (FEM) . . . 19
- 3.2 Meshless methods and enrichment functions . . . 20
- 3.3 Extended Finite Element Method (X-FEM) . . . 20
  - 3.3.1 Basic concepts . . . 20
  - 3.3.2 Basic formulation . . . 21
  - 3.3.3 Cracks located by level sets . . . 21

4 Numerical methods for cohesive crack propagation 23
4.1 Finite Element Method (FEM) . . . 23
4.2 Boundary Element Method (BEM) . . . 24
4.3 Meshless methods . . . 25

5 Thesis problem 27
5.1 Problem statement . . . 27
5.2 Variational formulation for cohesive crack model . . . 27
5.3 X-FEM approximation for cohesive crack model . . . 30
5.3.1 Formulation . . . 30
5.3.2 Cohesive zone mesh and integration . . . 30
5.3.3 Enrichment functions for cohesive crack model . . . 30
5.3.4 Crack propagation criterion . . . 30
5.3.5 Numerical algorithms . . . 31

6 Numerical studies 35
6.1 Code implementation . . . 35
6.2 Three point bending test . . . 35
6.2.1 Problem specification . . . 36
6.2.2 First results . . . 37
6.2.3 Mesh size and numerical accuracy . . . 40
6.2.4 Effect of different algorithms on the results . . . 43
6.2.5 Effect of crack propagation criteria on the results . . . 46
6.2.6 Effect of brittleness number . . . 46
6.2.7 Effect of initial cracks . . . 51
6.2.8 Apparent and real properties . . . 53

7 Conclusions 59
7.1 Conclusions . . . 59
7.2 Achievements and knowledge contribution . . . 60
7.3 Future works . . . 61

Bibliography 63

A C++ code implementation for numerical simulations 69
A.1 Input and output files . . . 69
A.1.1 Input files . . . 69
A.1.2 Output files . . . 73
A.2 Main files of the code . . . 74
A.2.1 main . . . 74
A.2.2 Mechanics . . . 75
A.2.3 xcCrack . . . 78
A.3 Xfem library . . . 79

A.3.1 Basic classes 79
A.3.2 New classes and functions 80
A.4 Xcrack library 80
A.4.1 Basic files and classes 80
A.4.2 New classes and functions 81

List of Figures **83**

Acknowledgements

The author acknowledges gratefully *Dr. Nicolas Chevaugeon* for his supervision on this thesis and also *Institut de Recherche en Génie Civil et Méchanique* (GeM) for supports.

Chapter 1

Introduction

Fracture mechanics is the systematic study of the crack propagation in solids. The establishment of fracture mechanics is closely related to catastrophic disasters happened in the recent history. During world war II many of liberty ships fractured even into two parts because of the choice of the brittle materials for the construction and also the stress concentrations in the faults existing in the welds. In July 1962 the Kings Bridge in Melbourne failed suddenly because of the propagation of fracture in four girders. The studies on the causes of such phenomena lead to progressive developments in fracture mechanics.

Existence and propagation of cracks in steel and concrete elements in civil engineering structures is quite important since it effects very much the ultimate mechanical strength and resistance of the structure to environmental effects. The study of the crack propagation is also quite important to estimate the ultimate strength and the failure procedures is such structures especially during earthquakes.

Fracture mechanics has now evolved into a mature discipline of science and engineering. One of its greatest impacts is on development of a new damage tolerance design methodology which is now used in aircraft design standards.

Brittle materials like high strength steel, glass, concrete, etc undergo brittle fracture the study of which is in the domain of *Linear Elastic Fracture Mechanics (LEFM)*. The main assumption for LEFM is that plasticity does not play an important role during fracture.

LEFM assumption is quite restrictive for certain types of failure in materials like structural steels though such materials can be prone to brittle fracture, which has lead to a number of catastrophic failures. Such materials show a quasi brittle or a ductile behavior for which plasticity plays an important role during the crack propagation and fracture.

Quasi brittle and ductile materials also render special behaviors like struc-

tural size effects on the material properties, strain softening and the ductile to brittle change of behavior of structures. Such behaviors are due to the damage localization in the area in front of the crack tip called *process zone*, prediction of which requires the consideration of the stress states in the process zone.

The facts mentioned above became the main motivation for development of a new field in fracture mechanics taking into account the plasticity in the process zone named *Elasto-Plastic Fracture Mechanics (EPFM)*. The simplest of such models is *cohesive crack model*.

During years numerical methods have been employed and regarded as suitable tools to predict the fracture and failure of engineering structures leading to creation of a science field called *computational fracture mechanics*. With the great advances in the field of science and engineering, the need to analyze larger and more complicated structures numerically has become an important issue for which development of the numerical tools and algorithms more efficient regarding the computational costs and the accuracy of the results is quite essential.

One of the most important difficulties is computational fracture mechanics is the fact that in mesh based numerical methods the mesh needs to conform to the geometry of the crack which requires a remeshing procedure during crack propagation which causes a high computational cost for large and complicated structures. Another difficulty is to increase the accuracy of the results near the crack tip which renders a singular behavior.

Cohesive crack model has been included in several numerical methods like boundary element method, mesh less methods and FEM. Different algorithms have been proposed to solve the nonlinearity of the problem coming from the process zone. Recently a new numerical method called *Extended Finite Element Method (XFEM)* has been developed. X-FEM uses the concept of partition of unity and enrichment functions to improve the accuracy of the problem and to include discontinuities in the problem. The first outcome of using X-FEM is that the mesh does not need to conform to the geometry of the problem any more. These properties can be used best in fracture mechanics for the aim of the crack propagation without remeshing and also to increase the numerical accuracy of the results around the crack tip.

The aim of this master thesis is to use X-FEM to solve cohesive crack propagation problems. In order to perform the numerical simulations a C++ code has been developed to include cohesive crack model in *Xfem* and *Xcrack* C++ libraries already developed in *Institut de Recherche en Génie Civil et Méchanique (GeM)*(Institute of research on civil and mechanical engineering) at *Ecole Centrale de Nantes (ECN)*. The numerical studies have been performed for a three point bending test. During the study, first, different algorithms and crack propagation criteria are discussed and their effect on the numerical accuracy and the robustness of the code is investigated. Next, using the most efficient algorithm,

an investigation on the efficiency of X-FEM regarding the computational costs and the numerical accuracy for solving cohesive crack propagation problems compared to other mesh based methods is performed. Finally using X-FEM with the most efficient algorithm, the capability of cohesive crack model to predict the size effects, strain softening and the ductile to brittle change of the behavior of the structure are investigated numerically.

According to the numerical results obtained, it is observed that using X-FEM the computational costs to obtain acceptable results are reduced very much compared to classical FEM. It is observed that using the algorithms proposed in the study, stress and SIF-I crack propagation criteria provide the same results for the same mesh. It is also observed that using cohesive crack model strain softening and the ductile to brittle change of the behavior of the structure can be captured. The size effects on the apparent tensile ultimate strength for a beam without an initial crack and apparent fracture toughness for a beam with an initial crack are also observed.

This master thesis report contains a detailed description of all the theoretical and numerical investigations performed by the author for his master thesis studies on numerical analysis of the cohesive crack propagation using X-FEM.

In chapter 2 a review on the theoretical background and the state of the art on fracture mechanics and cohesive crack model, required to follow the thesis is presented. In *fracture mechanics* section a brief insight from the theoretical concepts to analyze the behavior of the specimens with crack is presented. The difference between linear and nonlinear fracture mechanics is discussed and also some important concepts like process region, energy release rate, stress intensity factor and J-integral are introduced. Some material behaviors coming from the process region like strain softening and scale effects are also discussed. In *cohesive crack model* section, cohesive crack model as one of the simplest approaches to model the process region around the crack tip and its basic concepts and state of the art are presented. At the end the capability of this model to express scale effects as well as its limitations are discussed.

In chapter 3 a review on the theoretical background and also the state of the art on some numerical methods are presented. In section *Finite Element Method (FEM)*, the classical finite element method used for solid mechanics problems is introduced. The problems arising when FEM is used for problems with discontinuities and rough solutions like the existence and the propagation of crack and LEFM as well as some numerical methods developed to treat such problems are discussed in section *Meshless methods and enrichment functions*. Finally in section *Extended Finite element method (X-FEM)*, X-FEM as a numerical method having good characteristics of meshless methods to treat discontinuities and rough solutions while preserving the classical displacement variational settings and meshing concepts is introduced. In this section the basic concepts and

advantages of *level set technique* as an efficient way to locate cracks in the body are also presented.

In chapter 4 a state of the art on different numerical techniques used to model cohesive crack growth numerically is presented.

In chapter 5 the thesis problem is described. In *Variational formulation for cohesive crack model* section the variational formulation for cohesive crack model is developed. In *X-FEM approximation for cohesive crack model* section, the discretized version of the variational formulation for cohesive crack model using X-FEM is developed. In this section different crack propagation criteria as well as different algorithms to solve the nonlinear problem are also presented.

In chapter 6 the numerical results obtained for a three point bending test using cohesive crack model with the code implemented by the author of this thesis are presented. In *Code implementation* section a general overview on the code developed for numerical studies is presented. In *Three point bending test* section first the geometrical and mechanical parameters of the three point bending test together with boundary conditions are presented. Next the first results obtained are discussed and compared to the results obtained by *Carpinteri* and *Colombo* in [16]. Next a numerical study to show the efficiency of X-FEM regarding the mesh size compared to other methods is done. Finally the ability of cohesive crack model to express the ductile to brittle change of the behavior of the structure and also size effects as well as the effect of the existence of the initial cracks on the behavior of the beam are discussed according to the results obtained.

In chapter 7 the main conclusions of the present study as well as the achievements of the author from the study and the contribution of this study to knowledge and also the possible future works as the extension of this study are discussed.

In appendix A a brief summary on C++ code implementations used for the numerical simulations performed in the present study is presented. This appendix makes it easy for the user to use the code for other similar numerical investigations and also for the further developments of the code in the future. In *Input and output files* section the input files and parameters required by the code are presented and a brief description for each output file is also provided. In *Main files of the code* section the main C++ classes and functions developed for algorithm 2 in the present study are presented. In *Xfem library* and *Xcrack library* sections some of the basic C++ files and classes of Xfem and Xcrack libraries as well as the new classes and functions implemented by the author of this thesis for cohesive crack model are explained in brief.

This report is written using LaTeX software and the plots are obtained using *Gnuplot* plotting software. The figures are prepared using *Ipe* which is a free vector graphics editor for creating figures in PDF or EPS format.

Chapter 2

Fracture mechanics and cohesive crack model

2.1 Fracture mechanics

2.1.1 Linear Elastic vs Elastic Plastic Fracture Mechanics

Mechanical failure can happen due to corrosion, wear, plastic collapse, fracture, etc. The word fracture in quasi brittle materials can be interpreted mostly as unstable crack growth. Fracture Mechanics is then about the systematic approach concerning growth of pre-existing macroscopic cracks.

Fracture mechanics mainly has been a concern from 20th century. By introduction of new concepts such as stress intensity factor, critical stress intensity factor and energy release rate by *Irwin (1957)*, the foundation of *Linear Elastic Fracture Mechanics (LEFM)* was made. The concept of autonomy of the field near crack edge, introduced by *Barenblatt (1959)*, that is independence of processes near crack edge from material type and body and loading geometry, under some conditions, became the assumption under which all the concepts of LEFM developed. The key assumption for LEFM is that the size of process region (see section 2.1.3) in front of the crack tip is negligible compared to the structure or specimen dimension.

With the advances in the material technology, new and modern materials with more ductility and fracture toughness were developed for which the assumptions of LEFM was no longer valid. In such cases that the size of process region was not negligible compared to structure or specimen dimensions, LEFM could not be used to analyze the fracture process. In such materials *Elastic Plastic Fracture Mechanics (EPFM)* provided the solution. EPFM had its birth at 1960s and

early 1970s. The three papers of *J.R. Rice (1968)* made a considerable advance in EPFM. He idealized plastic deformation as a nonlinear elastic phenomena for mathematical purposes and was able to generalize the *energy release rate* for such materials. He expressed this in terms of a path independent contour integral called *J-Integral* which became a very efficient tool to treat energy problems in fracture mechanics.

2.1.2 Loading modes

In fracture mechanics a crack can be defined as a separation in material that may occur due to sliding or opening. Such separation is of order of micro structures in material, like in homogeneities. The type of loading conditions that make each of the types of crack are referred to as Mode I for opening and Mode II and III for sliding. In practical situations a loading condition with mixed mode happens while presence of each mode alone is mostly reserved for experimental cases. Figure 2.1 shows different loading modes.

2.1.3 Process region

Regardless of size of structure, the whole fracture process takes place in a small region that is near crack edge, called *process region*. This region contains very big loads and the fact that the fracture in this region happens due to micro separations and coalescences makes all continuum mechanics equations in this region fail [12, p. 23]. That's why the material behavior in this region can not be expressed by usual constitutive lows coming from continuum mechanics .

The size of process region compared to dimension of structure or specimen has a big effect on the fracture behavior of the material. As mentioned in section 2.1.1, LEFM can be used to analyze fracture processes with negligible size of

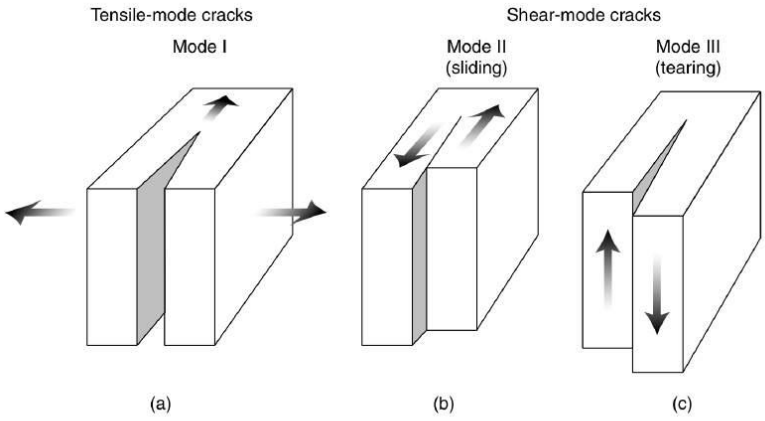

Figure 2.1: Different loading modes

cohesive zone compared to structure or specimen dimension (brittle materials). But in the cases where the size of cohesive zone is not negligible (i.e. quasi brittle or ductile materials), principles of LEFM can not be used any more and EPFM provides the solution.

2.1.4 Energy release rate

The crack propagation leads to dissipation of stress strain energy. This energy is dissipated in process region because of formation of micro separations and coalescences. *Irwin* was the first who observed that if the size of the plastic zone around crack tip is small compared to the size of the crack (i.e. brittle materials), the energy required to grow the crack will not be critically dependent on the state of stress at the crack tip [24]. Crack starts propagation when the energy coming from the stress- strain field is sufficient to support the formation of separations and coalescences. Strain energy release rate (or energy release rate) is then dissipated energy during fracture per unit of newly created fracture surface area [12, p. 33]. This quantity is central to fracture mechanics . For the purposes of calculation, the energy release rate is defined as

$$G = -\frac{dU}{da} \tag{2.1}$$

where U is the potential energy available for crack growth and a is the crack area. The units of G are $J/m2$. *Irvin* also adopted an additional assumption that the size and shape of the energy dissipation zone remains approximately constant during brittle fracture (LEFM assumption). According to this assumption the energy needed to create a unit fracture surface is a constant that depends only on the material. This quantity is called *fracture energy* (G_c) and is considered to be a material property which is independent of applied loads and the geometry of body. The crack propagation starts then when

$$G \geq G_c \tag{2.2}$$

2.1.5 Stress intensity factor

Since in LEFM model the state of stress near crack tip is singular, it is not possible to evaluate the stress value around crack tip accurately. In order to more accurately evaluate or predict the state of stress near crack tip *Irwin* and his colleagues developed a relation to calculate the amount of energy available for fracture in terms of asymptotic stress and displacement fields around a crack front in a linear elastic solid [26]. This asymptotic relation is:

$$\sigma_{ij} \approx \left(\frac{K}{\sqrt{2\pi r}}\right) f_{ij}(\theta) \tag{2.3}$$

where σ_{ij} are the Cauchy stresses, r is the distance from the crack tip, θ is the angle with respect to the plane of the crack and f_{ij} are functions that are independent of the crack geometry and loading conditions. The quantity K was called *Stress Intensity Factor*. Since functions f_{ij} are dimensionless, the stress intensity factor has the units of $MPa-\sqrt{m}$. This formulation is not valid for the areas very close to crack tip (small r) i.e. inside process region. This concept is a theoretical construct applicable to elastic materials and is useful for providing a failure criterion for brittle materials.

Stress intensity factor can be defined for different modes of loading (I, II and III) and in such cases is referred to as K_I, K_{II} and K_{III}. Stress intensity factors are related to energy release rate according to following equation for 2D problems:

$$G = \frac{K_I^2}{E^*} + \frac{K_{II}^2}{E^*} \tag{2.4}$$

where $E^* = E$ (Young's modulud) for plane stress and $E^* = E/(1-\nu^2)$ for plane strain problems (ν is the Poisson's ratio).

Stress intensity factor especially in mode one, can be used as a crack propagation criterion. There is a critical value for stress intensity factor, required to propagate the crack. This critical value determined for mode I loading in plane strain is referred to as *critical fracture toughness* (K_{Ic}).

2.1.6 J-integral

As mentioned in section 2.1.4, equation (2.1) is valid for materials for which the plastic zone around crack tip is small compared to the dimensions of structure or specimen (i.e. brittle materials). The $J-integral$ represents a way to describe the case where there is sufficient crack tip deformation that the part no longer obeys the linear elastic approximation. This analysis is limited to situations where plastic deformation at crack tip does not extend to the furthest edge of the loaded part. The theoretical concept of J-integral was developed in 1967 by *Cherepanov* [21] and in 1968 by *Jim Rice* [44] independently, who showed that an energetic contour path integral, called J, was independent of the path around a crack. This integral has the following general form:

$$J = \int_{\Gamma \cup \Gamma_{c^+} \cup \Gamma_{c^-}} \left(\frac{1}{2} \sigma_{ik} \epsilon_{ik} \delta_{1j} - \sigma_{ij} u_{i,1} \right) n_j \, ds \tag{2.5}$$

The coordinate system for this integral is local coordinate at crack tip with X_1 axis tangent to the crack at the tip. The scalar n_j is the j component of the outward normal to the closed path $\Gamma \cup \Gamma_{c^+} \cup \Gamma_{c^-}$ (See Figure 2.2 for notations). The physical meaning of J-integral is the power dissipated as the crack front advances with the velocity q. J-integral is related to stress intensity factors for

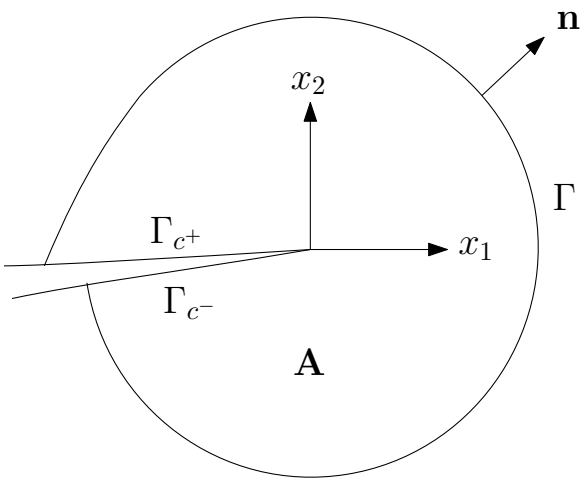

Figure 2.2: Notations for J-integral

different modes according to the following equation for two dimensional problems:

$$J = \frac{K_I^2}{E^*} + \frac{K_{II}^2}{E^*} \tag{2.6}$$

The elastic-plastic failure parameter is designated J_{Ic} and is conventionally related to K_{Ic} using the following equation:

$$K_{Ic} = \sqrt{E^* J_{Ic}} \tag{2.7}$$

In (2.6) and (2.7), E^* is the same as what in (2.4).

The J-integral is equal to the strain energy release rate for a crack in a body subjected to monotonic loading [50]. This is true, under quasi static conditions, both for linear elastic materials and for materials that experience small-scale yielding at the crack tip [12].

2.1.7 Strain softening and snap back phenomenon

Cracked solids often render an unstable behavior which is represented by a negative slope in load-deformation curves. Such behavior is called *strain softening* which means that in order to have a slow and stable crack propagation, the imposed load should be decreased. Such behavior is observed in both brittle and ductile materials. In the case of extremely brittle materials, crack propagation happens with a catastrophic drop of the load. This behavior is represented by a positive slope in the load-deflection curve if the loading process is displacement controlled. Such behavior is called *snap back phenomenon* which means that both load and displacement should be decreased. Figure 2.3 shows strain softening in both ductile and brittle materials.

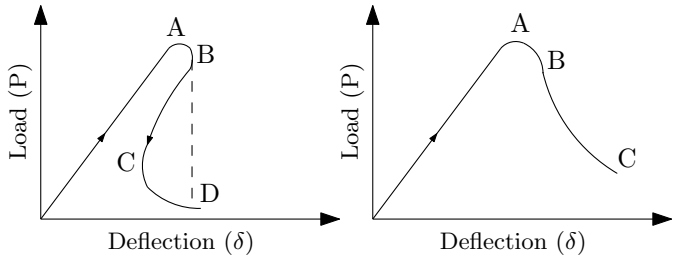

(a) Brittle material (snap back) (b) Ductile material

Figure 2.3: Strain softening in different materials

For the case of brittle material (snap back phenomenon), if the loading process is displacement controlled the experimental loading capacity will show a discontinuity with a negative jump. This jump is between point B and D in figure 2.3a. The branch BD in this figure will be then virtual. The catastrophic drop in the experimental loading capacity may be avoided and the snap back phenomenon can be experimentally shown if the values of load or displacement in the test vary with a parameter which is increasing monotonically (e.g. crack mouth opening, crack length, time).

Strain softening is due to the formation of micro cracking and coalescences and also localization of displacement in process region. From continuum mechanics point of view strain softening violates *Drucker's Postulate* [22] which states generally that the work of added stress should be always positive. This was pointed out first by *Maier* [30, 31] and *Maier et al.* [33].

2.1.8 Size effects

Size effects in fracture mechanics can be represented by the concept of nominal stress at failure:

$$\sigma_N = c_N \frac{P_u}{bd} \quad \text{for 2D problems} \qquad (2.8)$$
$$\sigma_N = c_N \frac{P_u}{d^2} \quad \text{for 3D problems}$$

where P_u is the maximum load, b is specimen thickness, d is the characteristic dimension of the specimen (e.g., its length or depth) and c_N is a parameter introduced for convenience [5]. It is well known that plastic limit analysis, as well as elastic analysis with an allowable stress criterion or any method of analysis with a failure criterion based on stress or strain exhibits the same nominal stress at failure for geometrically similar structures with different sizes. But experimental results show that such value is effected with the dimension of the structure or specimen. Such behavior is represented using fracture mechanics.

Size effects in Linear Elastic Fracture Mechanics

Total elastic energy of structures for two dimensional cases can be obtained according to the following formula:

$$U = \frac{\sigma^2 b d^2 f(\alpha)}{2E^*} \tag{2.9}$$

where $\sigma = c_N P/bd$ (P is load), E^* is the same as in (2.4) and $f(\alpha)$ is a function of crack length and shape of the specimen with $\alpha = a/d$ (a is the crack length). Considering equations (2.1) and (2.4) one will obtain:

$$K_I = \frac{Pk(\alpha)}{b\sqrt{d}} \tag{2.10}$$

where $k(\alpha) = [-f^{'}(\alpha)c_N^2/2]^{1/2}$. Taking into account (2.10) one will obtain

$$\sigma_N \propto d^{-1/2} \tag{2.11}$$

The same relationship can be obtained for 3D problems. As mentioned in previous sections, the assumption of LEFM will be true if the size of cohesive zone is negligible compared to dimensions of the structure or specimen.

Size effects in nonlinear fracture mechanics

Making the hypothesis that the energy dissipated at failure is a smooth function of both the specimen or structure size and the process zone width and that the latter is constant, *Bažant* [6] showed by dimensional analysis and similitude arguments that

$$\sigma_N = Bf_u\{\beta[1 + \beta^{-1} + A_1\beta^{-2} + A_2\beta^{-3} + \dots]\}^{-1/2}, \quad \beta = d/d_0 \tag{2.12}$$

in which B, d_0, A_1, A_2,... are empirical coefficients, f_u is some measure of tensile strength and β is a parameter characterizing the relative structure size. This equation represents an asymptotic expansion with respect to an infinitely large specimen. It was shown further in [7] that this relation can be truncated for size range of 1:20 and reduced to the size effect law proposed by *Bažant* [4, 5]:

$$\sigma_N = Bf_u\Big(1 + \frac{d}{d_0}\Big)^{-1/2} \tag{2.13}$$

It is clear from this equation that for values of $d \gg d_0$ the result is that of linear elastic formulation ($\sigma_N \propto d^{-1/2}$) while for values of $d \ll d_0$ the result is that of yield stress criterion (Bf_u). This fact is illustrated in figure 2.4.

In the cases where the size of process zone is not negligible compared to dimensions of the specimen or structure, the values of fracture toughness (K_{Ic}) and critical energy release rate (G_c) are highly effected by the size of structure

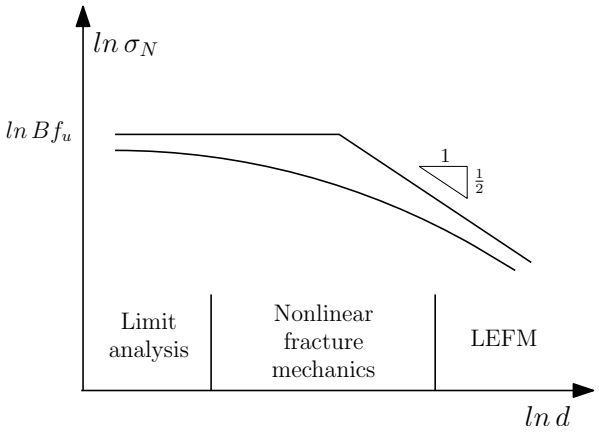

Figure 2.4: Bažant's size effect law

or specimen. In such cases, as proposed by *Bažant* [8, 9], the effective length of fracture process zone and critical energy release rate for a specimen of infinite size can be considered as material properties.

The elastic stress and displacement field surrounding a nonlinear process zone correspond to a certain crack length a. In this case one can write:

$$a = a_0 + c \tag{2.14}$$

where a_0 is the initial length on the notch or crack. Supposing that in corresponding linear elastic problem with crack length a the fracture growth under constant load is unstable, c represents the equivalent length on the nonlinear fracture process zone. For infinite large specimen or structure (i.e. $d \to \infty$), $c \to c_f$. c_f is called effective length of fracture process zone and is considered as a material property.

What mentioned up to now shows that the size of equivalent process zone, in front of crack tip, in fracture mechanics has a deterministic, although not exclusive, effect on the fracture behavior of the structure. If the size of equivalent process zone is negligible compared to specimen or structure dimensions, the fracture behavior will be that of linear elastic fracture mechanics (brittle), scale effects are according to (2.11) and as stated in previous sections critical energy release rate (G_c) and fracture toughness (K_{Ic}) are considered as material properties. If the size of equivalent process region is big compared to specimen or structure dimensions, the failure will be determined by strength or yield criterion (ductile). But if the size of equivalent process region is intermediate compared to dimensions of specimen or structure (quasi brittle), a ductile to brittle behavior is observed depending on the size of the structure according to (2.13).

The same discussion can hold for critical energy release rate (G_c). In this case for an infinite large specimen or structure $G_c \to G_f$. G_f is called *fracture energy* and is considered as a material property. According to [8, 9], (2.13) can

be written in terms of fracture energy and equivalent length of fracture process zone:

$$\sigma_N = c_N \left(\frac{E^* G_f}{g'(\alpha_0) c_f + g(\alpha_0) d} \right)^{1/2} \tag{2.15}$$

where $\alpha_0 = a_0/d$. In this formula the size effect is represented in terms of true material properties (c_f and G_f) and a function ($g(\alpha_0)$) which represents the geometry of structure or specimen.

2.2 Cohesive crack model

2.2.1 Modeling of fracture process region

As mentioned in previous sections, from the importance of process region in fracture mechanics, it is clear that most of the material behaviors like strain softening and size effects, are due to material behavior in this region and a model which takes into account the specific behavior of material in this very small region can represent such behaviors well. It should be noted again that LEFM does not take into account the material behavior in process region and as will be shown in numerical results in this study, is unable to show the behaviors coming from this region like strain softening in ductile materials.

In order to model process region, Finite Element Method has been used by so many people as a numerical tool. *Rashid* [43] used a model called *smeared crack model*. In this model there is an upper limit for stress (tensile strength of material). If the stress exceeds such value it is put to zero. So there is a drop of stress to zero after reaching the material tensile strength. *Scanlon* [46] used another constitutive model in which stress reduces to zero in a sequence of some drops.

So far strain softening has been added to Finite Element Method but there is a problem. The problem is that the energy dissipation through crack faces converges to zero by a mesh refinement. Such problem is called *spurious mesh sensitivity* and is not physically accepted. A solution to this problem is to specify the energy dissipated over crack surfaces. One of the physical approaches for doing so is by introducing a stress - crack opening constitutive relationship over crack surfaces in which the stress over crack surfaces decrease as the crack opening increases. Such method is the basis of a model called *cohesive crack model*.

The cohesive crack model was first proposed by *Barenblat* [2, 3] and *Dugdale* [23] . *Hillerberg et al.* [25] proposed the *fictitious crack model* in which the crack will propagate when the stress at the crack tip reaches the tensile strength. In his model the stresses applied on the crack surfaces decrease with the increase in crack opening and does not drop to zero suddenly. This fact makes the crack close smoothly and remains no singularity at the crack tip at the unset of crack

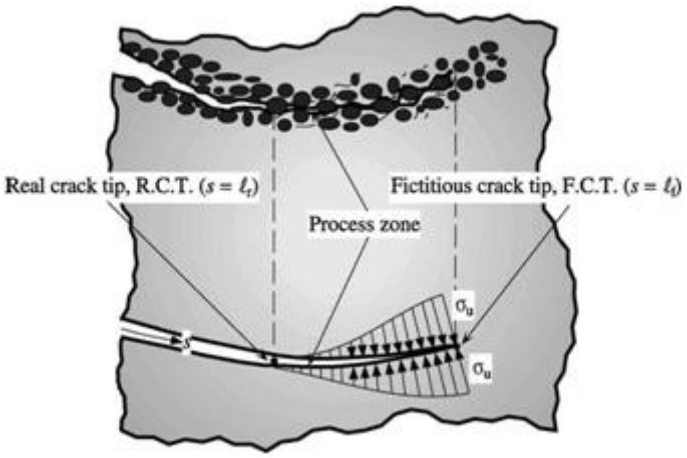

Figure 2.5: Process zone in cohesive crack model (figure from [17])

propagation which makes stress intensity factor in mode one (K_I) vanish. This fact and also the fact that evaluation of stress at crack tip is not accurate before the unset of crack propagation, inspired *N. Moës* and *T. Belytschko* [37] to use the value of K_I instead of the value of stress as a criteria for crack propagation.

Cohesive crack model was also used by *Carpinteri et al.* [16]. In order to explain size effects upon the parameters of cohesive crack model, they applied fractal geometry concepts and developed an improvement of cohesive crack model called (scale-invariant)*fractal cohesive crack model* (not studied in the present thesis) [17].

2.2.2 Basic concepts of cohesive crack model

In cohesive crack model, the process region is modeled as an extension of the crack length up to a point called *fictitious crack tip* (or *mathematical crack tip* in [37]). In this region (Figure 2.5) a specific constitutive law is considered while the linear elastic constitutive law is used for other regions. According to this specific law stress decreases with increase in crack opening according to a specific function. The *real crack tip* (or *physical crack tip* in [37]) is the point on the crack surface on which there is no stress i.e. the normal opening is bigger than the critical opening. One example of this constitutive law and the linear elastic constitutive law are shown in Figure 2.6.

The area under stress-crack opening curve represents fracture energy that is as explained in section 2.1.8 a material property. The following equation shows this property:

$$G_f = \int_0^{w_c} \sigma \, dw \tag{2.16}$$

Since in cohesive crack model the energy release rate is specified as a material parameter, there will be no spurious mesh sensitivity problem in the numerical solutions.

Thanks to the presence of stress on crack surfaces in process region, the crack will close smoothly and at unset of crack propagation there is no more singularity at crack tip which makes stress intensity factor in mode one (K_I) vanish. It should be noted that in this model the shear stresses on crack surfaces are neglected because of their small effect as is proved in [18].

2.2.3 Crack propagation criterion

Two approaches can be used to evaluate the unset of crack propagation. The first approach is to measure the principal stress at crack tip. The crack propagation happens then when the principal stress reaches the tensile strength of the material. The second approach is to use a criteria which evaluates the stress intensity factor for mode I (K_I). The unset of crack propagate then under the loading condition which makes K_I zero at the mathematical crack tip.

2.2.4 Size effects in cohesive crack model

Cohesive crack model is able to capture size effects in specimens or structures with high stress gradients (like three point bending tests). Uniaxial tests on dog-bone shaped specimens (with law stress gradients) show that the physical parameters characterizing cohesive crack model are scale-dependent. By increasing the size of the model, the tensile strength decreases while the fracture energy as well as critical crack opening increases. In these cases cohesive crack model is unable to capture size effects.

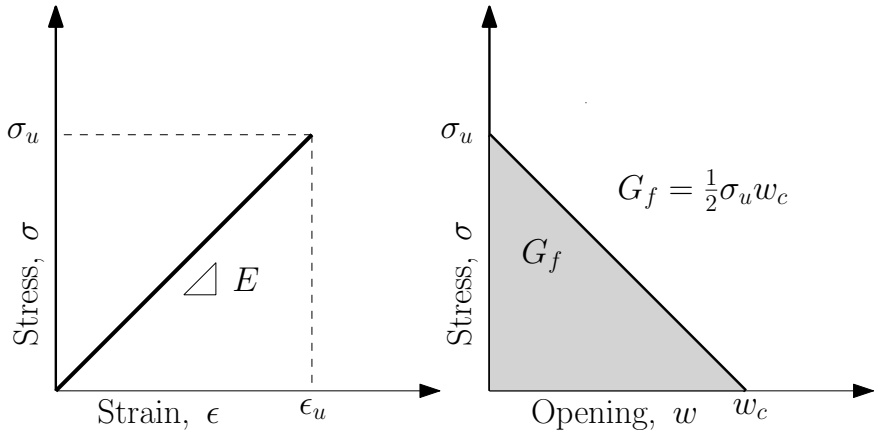

(a) Out of process region (b) Inside process region

Figure 2.6: Constitutive law inside and outside process region

The fact that size effects can be observed also in direct tension tests with bone shaped samples which have low stress gradient shows that there should be a reason for size effects other than stress gradient that comes from the material behavior. This problem was solved by a fractal approach leading to the *(scale invariant) fractal cohesive model* introduced by *Carpinterin et al.* [17].

2.2.5 Brittleness number

To compare the brittleness of different specimens, a non-dimensional number called *Energy Brittleness Number* has been introduced by *Carpinteri* [14].

$$s_E = \frac{G_f}{f_u b} = \frac{w_c}{2b} \tag{2.17}$$

In (2.17) b is the length scale of the specimen (it can be the hight of the beam in three point bending test), G_f is the fracture energy, f_u is the ultimate tensile strength of the material and w_c is the critical crack opening. The specimen renders a ductile behavior for high values of s_E while it renders brittle behavior for low values of s_E.

According to (2.17) not the single values of G_f, h and f_u, but their function s_E effects the ductile to brittle change of behavior of the structure. Hence a small structure or a structure made of a material with high G_f or low f_u has a ductile behavior while a large beam or a beam made of a material with low G_f or high f_u has a brittle behavior. This fact is more investigated in section 6.2.6.

Chapter 3

Numerical methods

3.1 Finite Element Method (FEM)

Finite element method is a numerical technique to solve partial differential equations (PDEs) as well as integral equations approximately. The equation will be defined over a domain Ω and will be discretized by FEM over some sub domains with simple geometry Ω_i called *finite elements* which are defined by their nodes. This fact is represented by the following equation.

$$\Omega = \cup_{e=1}^{N_e} \Omega_e \tag{3.1}$$

In (3.1), e refers to each element and N_e is the number of all elements in the domain. The set of elements constitute the mesh. The equation will be approximated through each element using functions called *shape functions* with respect to unknown *nodal values* (degrees of freedom). The shape functions are of polynomial type and fulfill the concept of *partition of unity* that is for each point x in the domain:

$$\sum_{i \in I} \phi_i(x) = 1 \tag{3.2}$$

where I is the set of all nodes in the domain and ϕ_i is the shape function associated to node i.

For solid mechanics problems, the equation to be solved is usually on the displacement (u) of the body. The classical FEM discretization then reads:

$$\mathbf{u}^h = \sum_{i \in I} \mathbf{u}_i \phi_i \tag{3.3}$$

where $\mathbf{u}^h$ is the approximated value of displacement, I is the set of all nodes, $\mathbf{u}_i$ is the vectorial degree of freedom (unknowns for each node) and ϕ_i is the associated shape function. Each shape function has a compact support (over which its value is other than zero) given by the union of the elements connected to node i.

3.2 Meshless methods and enrichment functions

There are some problems for which classical FEM approximation fails. Such problems are the ones whose solutions are rough (i.e. the derivatives of the solution (u) are not square integrable or they exist but are very large) or highly oscillatory. Another case is when there is discontinuity in the solution field. Examples of such cases are the singular state of stress close to crack tip and existence or propagation of cracks in fracture mechanics. In these cases the usual piecewise polynomial approximation spaces can not resolve the essential features of the solution unless the mesh size h is very small or the polynomial degree p is very large. In the cases like propagation of cracks a remeshing procedure is also required in order make the mesh conform with the geometry of the crack. In all such cases the computational costs are high.

In order to treat the problems with FEM, a numerical method called *meshless method* has been developed. Within the framework of meshless methods the support of the approximation function plays an important role and there exists no more elements. In this method if the behavior of the solution is known a priori, it can be incorporated directly into the numerical method [34] in the form of *enrichment functions*. In fact such concept allows us to include a priori knowledge about the problem under consideration in the finite element space through enrichment functions defined on the supports of approximation functions.

The concept of enrichment function has been used in many different numerical techniques under the category of meshless methods, having partition of unity property as the base. *Melenk* and *Babuška* [34] used such concept in *Partition of Unity Finite Element Method* (PUFEM) and applied it to *Helmholtz* equation which is a highly oscillatory problem. *Krysl* and *Belytschko* [28] also solved the problem of crack propagation in two and three dimensions without remeshing within the framework of *Element Free Galerkin Method*, using discontinuous functions on the crack and singular enrichment functions on the crack tip.

3.3 Extended Finite Element Method (X-FEM)

3.3.1 Basic concepts

The concept of enrichment functions in meshless methods, was used in classical finite element (with mesh) by *T. Belytschko*, *N. Moës* and *J. Dolbow* [10, 35]. This extension of FEM was called *eXtended Finite Element Method* (X-FEM). X-FEM allows local enrichment functions to be incorporated into a finite element approximation while preserving the classical displacement variational settings and meshing concepts.

X-FEM best suits the crack propagation problems. Thanks to discontinuous enrichment functions, using such method, since the mesh does not need to

conform to the problem geometry, there is no need for remeshing during crack propagation.

3.3.2 Basic formulation

For solid mechanics problems, the equation to be solved is usually on the displacement (u) of the body. The X-FEM discretization then reads:

$$\mathbf{u}^h = \sum_{i\in I} \mathbf{u}_i \phi_i + \sum_{j\in J} \mathbf{b}_j \phi_j H\big(f(x)\big) + \sum_{k\in K} \phi_k \Big(\sum_{l=1}^{4} \mathbf{c}_k^l F_l(x) \Big) \tag{3.4}$$

In (3.4) the last two terms on the r.h.s. are the terms associated to enrichment functions. The function H is the jump function and is used to introduce discontinuity in crack faces. It has the following formulation:

$$H(x) = \begin{cases} -1 & \text{if } x > 0 \\ 1 & \text{if } x < 0 \end{cases} \tag{3.5}$$

$f(x)$ can be any function showing the side of the crack where x is located and can be the signed distance function to the crack. F_l are enrichment functions (branch functions) used to increases the accuracy of the numerical solution around crack tip and their formulation is dependent on the nature of the problem to be solved. For LEFM problems these functions are chosen based on the asymptotic behavior of the displacement field at the crack tip:

$$\{F_l(r,\theta)\} \equiv \left\{ \sqrt{r}\sin\left(\frac{\theta}{2}\right), \sqrt{r}\cos\left(\frac{\theta}{2}\right), \sqrt{r}\sin\left(\frac{\theta}{2}\right)\sin(\theta), \sqrt{r}\cos\left(\frac{\theta}{2}\right)\sin(\theta) \right\} \tag{3.6}$$

where (r,θ) are the local polar coordinates with respect to the crack tip.

In (3.4) I is the set of all nodes in the mesh, J is the set of nodes in the mesh whose shape function support is completely cut by the crack. K is the set of nodes enriched by the crack tip enrichment functions which are at least the nodes whose shape function supports include the crack tip. This type of enrichment is called *Topological Enrichment*.

The problem with Topological Enrichment is that the enriched zone will tend to zero when the mesh becomes finer which reduces the effect of tip enrichment functions on accuracy of the results. There is another approach called *Geometrical Enrichment* in which the nodes which are in an specific distance from the crack tip are enriched. This approach will lead to more accurate numerical results.

3.3.3 Cracks located by level sets

One can define a function over some points of a domain so that the isovalue contours of such function can represent the points on an special curve. This

approach is the base of a method called *level set technique*. Level set technique is a way to represent curves implicitly. Different functions can be used in level set technique and the most simple one is distance function. Using distance function the distance of points of a domain from a special curve can be defined and the curve can be located as the isozero contour of the distance function.

Level set techniques can be used efficiently to locate cracks for numerical purposes. In this approach, as proposed by [47] in 2D and by [36] in 3D, the crack can be defined by two levels sets. The first level set is the distance of points from the tangent line to the crack face (ls_n) and the second one is the distance from a line perpendicular to the crack at the crack tip (ls_t). The crack is then defined as the set of the points for which $ls_n = 0$ and $ls_t \leq 0$ and the crack tip is defined the point for which $ls_n = ls_t = 0$. Such representation of crack is suitable for the numerical methods where enrichment functions are used, since it makes it also easy to obtain polar coordinates of points with respect to crack tip, used in enrichment functions, according to following formulations [36]:

$$r = (ls_t^2 + ls_n^2)^{1/2} \quad \theta = \arctan\left(\frac{ls_n}{ls_t}\right) \tag{3.7}$$

Chapter 4

Numerical methods for cohesive crack propagation

4.1 Finite Element Method (FEM)

Different methods have been developed to model the cohesive crack propagation with FEM. Generally two approaches have been used for the crack propagation.

The first approach to model the crack propagation in FEM is *interelement* approach. In this approach the crack is modeled between element interfaces. This approach have been used for both brittle and ductile materials by many researchers. *A. Carpinteri* [15, 16, 17, 18] has used this approach to apply cohesive crack model to analyze the crack stability in elastic-softening materials like concrete. In his model they used the value of the principal stress as the crack propagation criterion in cohesive crack model. *Xu* and *Needleman* [48] and *Ortiz* and *Camacho* [13] also placed a cohesive zone between each pair of the neighboring elements to model the cohesive crack propagation.

The second approach to model crack propagation in FEM is *intraelement* approach. This approach essentially consist of enriching the continuous displacement modes of the standard finite elements, with additional discontinuous displacements, devised for capturing the physical discontinuity i.e.: fractures, cracks, etc. The discontinuity path is placed inside the elements irrespective of the size and specific orientation of them. As for the enriching technique, two approaches can be distinguished in terms of the support of the enriching discontinuous displacement modes. Below a brief description of each approach is presented. A comparative study on these approaches also can be found in [39].

Elemental enrichment: In these methods the support of each mode is an element which means that discontinuous mode are incorporated on an element

level. This approach requires the crack to propagate one element at a time. This approach has been used in [29] to model the crack propagation in concrete structures and also in [38] to model strong discontinuities in solids. A comparative study on different methods using this approach is performed in [27].

Nodal enrichment: In these methods the support of each mode is the same as the support of FEM shape functions i.e. the elements sharing an specific node. These methods generally use the concept of partition of unity to include the enrichment functions and are known with the name of *Extended Finite Element Method (X-FEM)*. For a brief description of X-FEM see section 3.3. X-FEM has been used for cohesive crack propagation by *Nicolas Moës* and *Ted Belytschko* in [37]. In their work they used the value of the stress intensity factor in mode I (k_I) as a more trusted criterion for crack propagation. In their model the crack path need not to be known in advance and the crack propagates when the value of (k_I) at the mathematical crack tip is zero. In their model the crack path is determined using the *maximum hoop stress criteria* and LEFM. They represented the process zone as 1-D segments and made a loop on cohesive zone length and the load to solve the nonlinear problem.

4.2 Boundary Element Method (BEM)

Boundary element method has been extensively used specially in fracture mechanics. Such method is attractive since it just needs the boundary of the domain to be meshed which results in a smaller stiffness matrix, although full and nonsymmetric, compared to FEM. Such property enables BEM to handle the crack propagation problems without remeshing. BEM has been used by many researchers to model cohesive crack growth among them the works of the following are mentioned here.

A. L. Saleh and *M. H. Aliabadi* [45] used *Dual Boundary Element Method (DBEM)* to model mode I and mixed mode nonlinear (cohesive) crack propagation in concrete. In their model the crack path need not to be known in advance and the crack propagates when the stress value at the crack tip reaches the maximum tensile strength of the material, in the direction perpendicular to the maximum principal stress. In order to get the proper length of the process zone, an iteration is defined over the load and the length of the process zone.

B. Yang and *K. Ravi-Chandar* [49] used a *single-domain dual-boundary-element* formulation as a boundary element approach to model the cohesive crack growth. In their formulation a cohesive zone is incorporated in the formulation resulting in a nonlinear problem. They also incorporated the local unloading effect on the cohesive zone. In their model the stiffness of the softening stress-crack opening model in the process zone is not non a priori and is obtained as a part

of the solution. Such nonlinear problem is solved using *successive-over-relaxation* iterative method. They also have taken into account the tangential interaction of the crack surfaces. In their model also, the crack propagates when the maximum principle stress is reached and the crack path is perpendicular to the maximum principle stress.

Other researchers who have used BEM for cohesive crack growth are *Z. Cen* and *G. Maier* who used *Multi Domain Boundary Element Method* [19] and also *Symmetric Galerkin boundary element method* [32] and *Chen et al.* who used *Multi-zone boundary element method* [20].

4.3 Meshless methods

Traditional simulation algorithms rely on a grid or a mesh, while meshfree methods use the geometry of the simulated object directly for calculations. This fact and also the fact that the a priori known behavior of the problem can be included in the solution using the concept of enrichment functions make meshless methods an attractive choice to handle the crack propagation in fracture problems. Different meshless methods have been used by many researchers to model the cohesive crack growth among them the works of the following are mentioned here.

T. Belytschkoa [11] used the *Element-Free Galerkin (EFG)* method to simulate the mixed-mode dynamic crack propagation in concrete. The EFG methodology allows for arbitrary crack growth in terms of direction and speed. They also included cohesive crack model in EFG and performed mode I and mixed-mode numerical tests on three point bending tests on a concrete beam with satisfactory results.

Timon Rabczuk and *Goangseup Zi* [42] developed a so called *Extended Element-Free Galerkin (XEFG)* method which is a meshfree method based on a meshfree concept of X-FEM using the local partition of unity for the cohesive cracks. In their model the crack propagation is governed by the material stability condition. Using the concept of enrichment functions they obtained very accurate results with higher smoothness and higher order of continuity which resulted in obtaining a better stress distribution around the crack tip compared to X-FEM. They also obtained nonlinear crack opening in the process region that is closer to the reality.

Chapter 5

Thesis problem

5.1 Problem statement

As mentioned in chapter 4 different numerical approaches has been developed and used by different researchers to model cohesive crack propagation. The aim of this thesis is to use X-FEM to solve cohesive crack propagation problems. For this aim the model proposed by *Nicolas Moës* and *Ted Belytschko* in [37] is used.

In order to perform the numerical simulations, a C++ code has been developed to include cohesive crack model in *Xfem* and *Xcrack* C++ libraries already developed in *Institut de Recherche en Génie Civil et Méchanique (GeM)*(Institute of research on civil and mechanical engineering) at *Ecole Centrale de Nantes(ECN)*.

During the study, first, different algorithms and crack propagation criteria are discussed and their effect on the numerical accuracy and the robustness of the code is investigated. Next, using the most efficient algorithm, an investigation on the efficiency of X-FEM regarding the computational costs and the numerical accuracy for solving cohesive crack propagation problems compared to other mesh based methods is performed. Finally using X-FEM with the most efficient algorithm, the capability of cohesive crack model to predict the size effects, strain softening and the ductile to brittle change of the behavior of the structure are investigated numerically.

5.2 Variational formulation for cohesive crack model

In this section the variational formulation for cohesive crack model as proposed by *N. Moës* and *T. Belytschko* in [37] is presented.

Consider a domain with geometry and boundary conditions shown in figure 5.1. In this figure $\Gamma_{\mathbf{u}}$ represents the boundary of the domain on which essential (Dirichlet) boundary conditions are applied, $\Gamma_{\mathbf{F}}$ represents the boundary of the

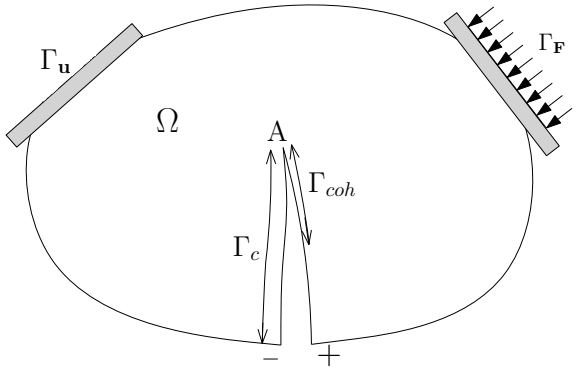

Figure 5.1: Domain and notations for specimen with cohesive crack

domain on which forces are applied and Γ_c and Γ_{coh} represent the crack surface and part of the crack surface that is considered as process region, respectively.

Assuming cohesive forces ($\mathbf{t}$) in process region (cohesive zone) (see figure 5.2), the general equilibrium equation in strong form for the domain reads:

$$\begin{aligned} &\nabla \cdot \boldsymbol{\sigma} = 0 \quad \text{on } \Omega, \quad \boldsymbol{\sigma} \cdot \mathbf{n} = \mathbf{F} \quad \text{on } \Gamma_F \\ &\boldsymbol{\sigma} \cdot \mathbf{n}^+ = -\boldsymbol{\sigma} \cdot \mathbf{n}^- = \mathbf{t}^+ = -\mathbf{t}^- = \mathbf{t} \quad \text{on } \Gamma_{coh} \end{aligned} \tag{5.1}$$

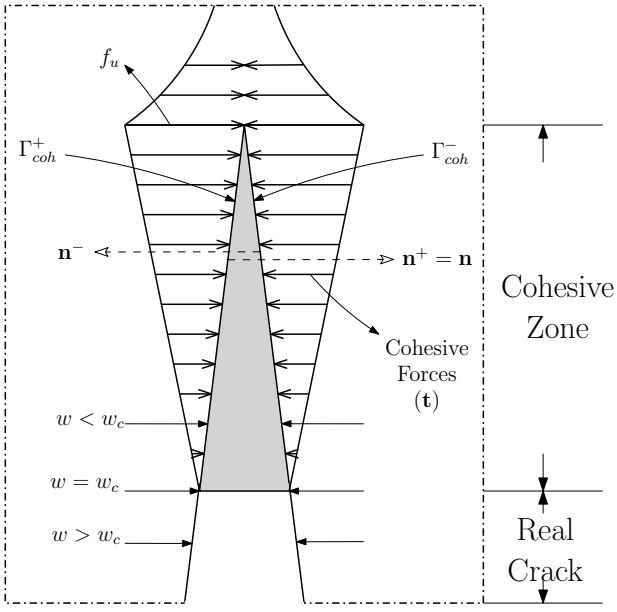

Figure 5.2: A zoom in cohesive zone

With small strain assumption in the domain, the kinematic equation reads

$$\begin{aligned} \boldsymbol{\epsilon} &= \frac{1}{2}\left(\nabla \mathbf{u} + (\nabla \mathbf{u})^T\right) \equiv \boldsymbol{\epsilon}(\mathbf{u}) \quad \text{on } \Omega, \quad \mathbf{u} = 0 \quad \text{on } \Gamma_u \\ \mathbf{w} &= \left(\mathbf{u}^- - \mathbf{u}^+\right) \quad \text{on } \Gamma_{coh} \end{aligned} \tag{5.2}$$

As already stated, in cohesive crack model, two constitutive laws for the material will be assumed: linear elastic outside process region and a softening stress - crack opening law in process region. These constitutive laws are:

$$\begin{aligned} \boldsymbol{\sigma} &= \mathbf{C} : \boldsymbol{\epsilon} \quad \text{on } \Omega \\ \mathbf{t} &= \mathbf{t}(\mathbf{w}) \quad \text{on } \Gamma_{coh} \end{aligned} \tag{5.3}$$

The weak form of the equilibrium equation, better suited for finite element analysis, now reads:

$$\int_\Omega \boldsymbol{\sigma} : \boldsymbol{\epsilon}(\mathbf{v})\, dx = \int_{\Gamma_F} \mathbf{F} \cdot \mathbf{v}\, ds + \int_{\Gamma^+_{coh}} \mathbf{t}^+ \cdot \mathbf{v}\, ds + \int_{\Gamma^-_{coh}} \mathbf{t}^- \cdot \mathbf{v}\, ds \quad \forall \mathbf{v} \in \mathcal{U} \tag{5.4}$$

where $\mathcal{U}$ is the *kinematically admissible* displacement field:

$$\mathcal{U} = \{\mathbf{v} \in \mathcal{V} : \mathbf{v} = 0 \text{ on } \Gamma_u\}$$

Them mathematical nature of $\mathcal{V}$ depends on the regularity of the solution. It allows for discontinuous displacement across crack faces (Γ_c). Using the notation $\mathbf{t}^+ = -\mathbf{t}^- = \mathbf{t}$ and $\mathbf{w} = \left(\mathbf{v}^- - \mathbf{v}^+\right)$ equation (5.4) becomes:

$$\int_\Omega \boldsymbol{\sigma} : \boldsymbol{\epsilon}(\mathbf{v})\, dx + \int_{\Gamma_{coh}} \mathbf{t} \cdot \mathbf{w}(\mathbf{v})\, ds = \int_{\Gamma_F} \mathbf{F} \cdot \mathbf{v}\, ds \quad \forall \mathbf{v} \in \mathcal{U} \tag{5.5}$$

Different softening constitutive laws can be used for $\mathbf{t}(\mathbf{w})$ among which a linear one with slope $-k$ is selected for the present study (see figure 5.2):

$$f = f_u - kw \tag{5.6}$$

where $f = \mathbf{t} \cdot \mathbf{n}$ and $w(\mathbf{v}) = \mathbf{w}(\mathbf{v}) \cdot \mathbf{n}$ is the normal crack opening. Using this constitutive law for $\mathbf{t}(\mathbf{w})$ and linear elastic law for the domain outside the process region, (5.5) becomes:

$$\int_\Omega \mathbf{C}\boldsymbol{\epsilon}(\mathbf{u}) : \boldsymbol{\epsilon}(\mathbf{v})\, dx - \int_{\Gamma_{coh}} kw(\mathbf{u})w(\mathbf{v})\, ds = \int_{\Gamma_F} \mathbf{F}\cdot\mathbf{v}\, ds - \int_{\Gamma_{coh}} f_u w(\mathbf{v})\, ds \quad \forall \mathbf{v} \in \mathcal{U} \tag{5.7}$$

In the numerical algorithms (5.7) will be used as the variational formulation of the problem.

5.3 X-FEM approximation for cohesive crack model

5.3.1 Formulation

If (3.4) is used for discretization of (5.7), it becomes:

$$\int_{\Omega} \mathbf{C}\boldsymbol{\epsilon}(\mathbf{u}^h) : \boldsymbol{\epsilon}(\mathbf{v})\, dx - \int_{\Gamma_{coh}} kw(\mathbf{u}^h)w(\mathbf{v})\, ds = \lambda \int_{\Gamma_F} \mathbf{F}_0 \cdot \mathbf{v}\, ds - \int_{\Gamma_{coh}} f_u w(\mathbf{v})\, ds \quad \forall \mathbf{v} \in \mathcal{U}^h \tag{5.8}$$

Note that for numerical purposes, scalar λ (load factor) in (5.8) is used multiplied to a constant load vector $\mathbf{F}_0$.

5.3.2 Cohesive zone mesh and integration

In (5.8) the integration over domain (Ω) is done element by element. For integration over cohesive zone (Γ_{coh}) in 2D problems, this region is considered as 1D segments whose length can be independent of the size of the global mesh (user defined). In order to integrate asymptotic functions on these elements, four Gauss points may be selected for eahc element. In (5.8), the exact length of cohesive zone is not known a priori. In fact such length is one of the unknown variables of the problem and will be obtained from the solution. This fact introduces a nonlinearity in the crack propagation problem.

5.3.3 Enrichment functions for cohesive crack model

According to the asymptotic analysis of the displacement field in the process region of large scale structures provided in [40, 41] the following non-singular branch functions can be used as enrichment function:

$$\{F_l(r,\theta)\} \equiv r\sin\left(\frac{\theta}{2}\right) \quad \text{or} \quad r^{3/2}\sin\left(\frac{\theta}{2}\right) \quad \text{or} \quad r^2\sin\left(\frac{\theta}{2}\right) \tag{5.9}$$

Note that in the present study $r\sin(\frac{\theta}{2})$ is used as enrichment function.

5.3.4 Crack propagation criterion

In order to find the value of load for the unset of crack propagation (critical load), two approaches have been proposed in the literature. The first approach is to measure the value of stress at fictitious crack tip. The crack will propagate then when this value reaches the tensile strength of the material (stress criterion). The second approach, proposed by *N. Moës* and *T. Belytschko* in [37], is to measure the stress intensity factor in mode I (K_I). The crack will propagate then when this value is equal to zero (SIF-I criterion). This fact is a natural outcome of cohesive crack propagation. Since this approach uses energy considerations instead of point wise values to obtain unset of crack propagation, it may be trusted more. In numerical results section both criteria will be used and compared to each other.

5.3.5 Numerical algorithms

In this study we are interested to find critical state of the structure using cohesive crack model which means to find the values of load for which the state of the crack is critical (i.e. the crack is at its unset of propagation). For a problem with a specific geometry and boundary conditions, the problem will be to find values of load and cohesive length for which the crack propagation criterion will be fulfilled. Different algorithms can be developed to solve such nonlinear problem. In the following, different algorithms developed to solve the problem in the present study are presented. Note that in chapter 6 the efficiency of these algorithms are compared. Note also that these algorithms are developed for pure mode I problems where crack propagation direction is known a priori and the crack is linear. For the cases for which the crack propagation direction is not known a priori, the same algorithms may be used with small modifications to take into account computation of crack propagation direction.

Algorithm one

In this algorithm the critical load and cohesive zone length for each total crack length (i.e. real part and cohesive part) is calculated. The total crack length is increased step by step until a maximum total length is reached. In the following, the steps of algorithm 1 are presented:

1. Consider an initial total crack length (real part and cohesive part)
2. Consider the total crack length as cohesive zone and go to step 4.
3. Consider the length obtained for cohesive zone for previous total crack length as cohesive zone of this total crack length.
4. Solve the problem using (5.8) for two arbitrary load factors (λ_1 and λ_2). Obtain the load factor (λ_3) for which the crack propagation criterion (stress criterion or SIF-I criterion) is fulfilled. Note that since for a constant cohesive zone length, the problem is linear, λ_3 can be obtained exactly using a linear extrapolation.
5. Check the crack opening for the last 1-D segment in the cohesive zone away from fictitious crack tip. If the crack opening in all Gauss points is bigger than the critical crack opening, remove this element from the cohesive zone and go to step 4.
6. The solution for this crack length is obtained. Increase the total crack length in the crack propagation direction. If any 1-D element has been removed in step 5 during the whole iteration, go to step 3, otherwise go to step 2.

This algorithm is also used in [45] with a stress criterion for crack propagation. Figure 5.3 shows algorithm 1 schematically.

Algorithm two

This algorithm is proposed in this study. In this algorithm the critical load and cohesive zone length for each real crack length is calculated. The real crack length is increased step by step until a maximum real crack length is reached. In the following, the steps of algorithm 2 are presented:

1. Consider an initial real crack length.
2. Assume a value for the length of cohesive zone and go to step 4.
3. Consider the length obtained for cohesive zone for previous real crack length as cohesive zone of this real crack length.
4. Solve the problem using (5.8) for two arbitrary load factors (λ_1 and λ_2). Obtain the load factor (λ_3) for which the crack propagation criterion (stress criterion or SIF-I criterion) is fulfilled. Note that since for a constant cohesive zone length, the problem is linear, λ_3 can be obtained exactly using a linear extrapolation.
5. Check the crack opening for the last 1-D segment in the cohesive zone away from fictitious crack tip. If the crack opening in all Gauss points is bigger than the critical crack opening, remove the element containing the fictitious

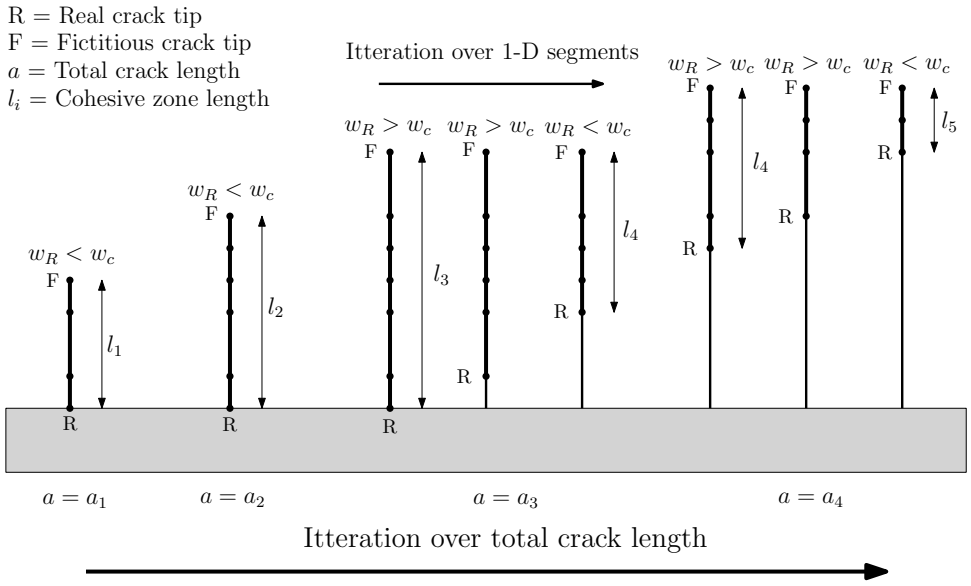

Figure 5.3: Algorithm 1 for cohesive crack propagation

crack tip and move the fictitious crack tip to the last segment remained and go to step 4. If the crack opening in one or some Gauss points is less than the critical crack opening, add a 1-D element after the element containing the fictitious crack tip and move the fictitious crack tip to the last vertex (away from real crack tip) of the added element and go to step 4. In order to avoid infinite loop, if the procedure of adding and removing an element is performed after each other once, skip the loop.

6. The solution for this real crack length is obtained. Increase the real crack length in the crack propagation direction. Go to step 3.

Figure 5.4 shows algorithm 2 schematically.

Algorithm three

In this algorithm the critical load and cohesive zone length for each total crack length (i.e. real part and cohesive part) is calculated. The total crack length is increased step by step until a maximum total length is reached. In the following, the steps of algorithm 3 are presented:

1. Consider an initial total crack length (real part and cohesive part)

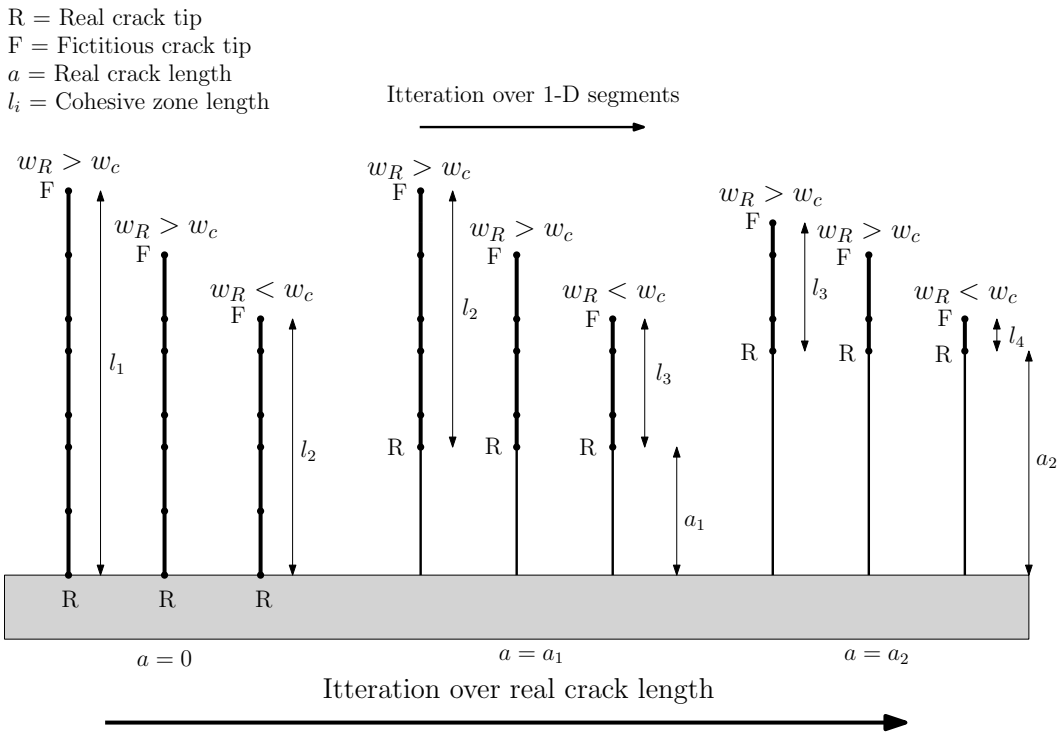

Figure 5.4: Algorithm 2 for cohesive crack propagation

2. Consider the total crack length as cohesive zone.
3. Solve the problem using (5.8) for a given load factor.
4. Check the crack opening for the last 1-D segment in the cohesive zone away from crack tip. If the crack opening in all Gauss points is bigger than the critical crack opening, remove this element from the cohesive zone and go to step 3.
5. Check if the crack propagation criterion is fulfilled within some user defined tolerance. If it is fulfilled go to step 6. If it is not fulfilled update the load factor using a secant method and go to step 3.
6. The solution for this crack length is obtained. Increase the total crack length in the crack propagation direction. Go to step 2.

This algorithm is proposed in [37] with SIF-I criterion for crack propagation.

Comparison between algorithms

In algorithm 1 and 3 the length of the real part of the crack is not under control and user defined. So these algorithms are not suited for studies on specimens having an initial real crack with an specific length. In fact in these algorithms the total length of the crack is under control. In contrary in algorithm 2 the length of the real part of the crack is under control and user defined. So this algorithm is suited for studies on specimens having an initial real crack with an specific length. In fact in this algorithm the maximum cohesive zone length will be obtained for each real crack length.

In algorithms 1 and 2, the fact that the loop on the load factor is performed for a crack with a constant length of cohesive zone makes it possible to obtain the exact value of the critical load factor using linear extrapolation. But in algorithm 3 such value is obtained from the solution of a nonlinear problem using secant method which renders a residual error that should be controlled.

Chapter 6

Numerical studies

6.1 Code implementation

The code implementation for cohesive crack model for the numerical studies has been done using C++ language. The code is developed on top of *X-FEM* C++ library which provide the routines for Extended Finite Element Method to solve the numerical problem and *X-Crack* C++ library which provides the level set means to locate cracks and crack propagation and also the numerical algorithms to compute J-integral and stress intensity factors at crack tip. Both libraries have been developed in *Institut de Recherche en Génie Civil et Méchanique (GeM)*(Institute of research on civil and mechanical engineering) at *Ecole Centrale de Nantes (ECN)*.

The library used for solving the system of equations is *SuperLU* which is a general purpose library for the direct solution of large, sparse, nonsymmetric systems of linear equations. The library routines perform an LU decomposition with partial pivoting and triangular system solves through forward and backward substitutions. The library is written in C.

Some details on input and output parameters of the code as well as some of the most important functions and classes defined in C++ for the code implementation are provided in appendix A.

6.2 Three point bending test

In this section the numerical results obtained for a three point bending test are presented. The crack propagation mode in this case is pure mode one hence the crack is planer and the crack initiation point and the crack path are known a priori.

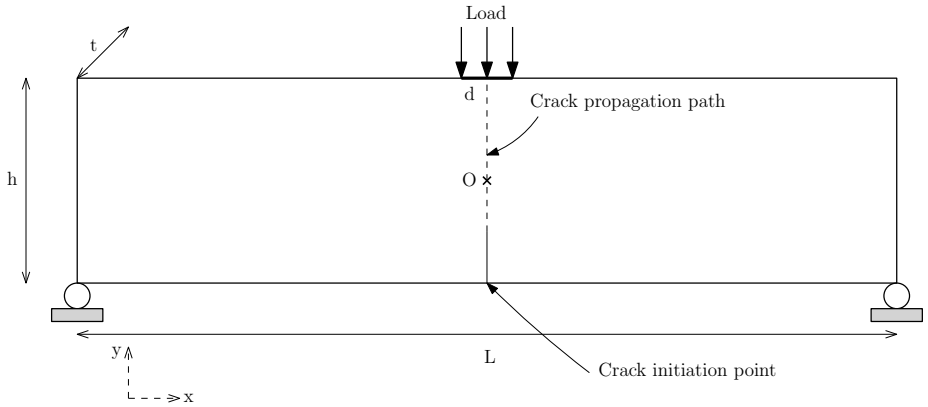

Figure 6.1: Geometry and boundary conditions of the three point bending test

6.2.1 Problem specification

Figure 6.1 shows the geometry, the crack location, the crack initiation point and the boundary conditions of the three point bending problem. Note that in order to avoid singular values of stress at the point of load application, the load is distributed over a length d, as is also the case in the reality. Note also that in order to avoid rigid body motion in the beam there are constraints for displacement of the beam in y direction at its supports and in x direction at point O (center of the beam).
The geometrical parameters of the beam are:

$$t = h = 150\,\text{mm}, \quad L = 4h = 600\,\text{mm}, \quad d = 10\,\text{mm} \tag{6.1}$$

The material used for simulation is concrete with the following mechanical properties:

$$E = 36500\,\text{MPa}, \quad \nu = 0.1, \quad f_u = 3.19\,\text{MPa} \tag{6.2}$$

There is initially no crack in the beam. As the force is increased the stress value at point of crack initiation will increase linearly until it reaches the tensile strength of the material. After that the cohesive zone starts to develop at this point until the crack opening becomes more than its critical value. The behavior of the beam becomes nonlinear at this level. Increasing the load at this state will cause a real crack propagation.

The beam is analyzed with plain strain assumption. Cohesive crack propagation of such specimen with the same geometrical and mechanical parameters has been extensively analyzed by *Carpinteri* and *Colombo* in [16] using a plane stress assumption and using a point load. Since the difference of plane stress and plane strain assumptions is the factor $(1 - \nu^2)$ in Young's Modulus (see (2.4)), the difference of these two assumptions is small for small values of Poisson ratio ($\nu = 0.1$).

6.2.2 First results

The first numerical results have been obtained for materials with $G_f = 50\,Nm^{-1}$ ($s_E = 1e^{-4}$) and $G_f = 5\,Nm^{-1}(s_E = 2e^{-5})$ (see (2.17)) using algorithm 2 with SIF-I criterion. Figure 6.2 shows the undeformed mesh and deformed shape of the beam together with the values of stress in X direction. The complete length of the crack (real part and cohesive part) can be seen in the middle of the beam.

It is observed from figure 6.2 that the mesh does not need to conform to the geometry of the crack thanks to discontinuous enrichment functions used in X-FEM. It is also observed that the crack closes smoothly thanks to the presence of tensile stresses on crack faces. As is clear from this figure, the value of stress in X direction (which is the principal direction for this problem) is equal to the tensile strength of the material $f_u = 3.19$.

Figure 6.3 shows the non-dimensional load-deflection curves obtained for the two values of G_f and also the curves obtained by *Carpinteri* and *Colombo* in [16]. In this figure m is number of elements on the height of the beam h in the center of the beam span. It is observed that the results obtained by X-FEM for $m = 19$ are very close to the results obtained by *Carpinteri* and *Colombo* in [16] for $m = 40$.

Figure 6.4 shows an example of the output tables made by the code for $G_f = 50\,Nm^{-1}(s_E = 1e^{-4})$ using algorithm 2 with SIF-I criterion. The units of parameters in the table are $N - mm$.

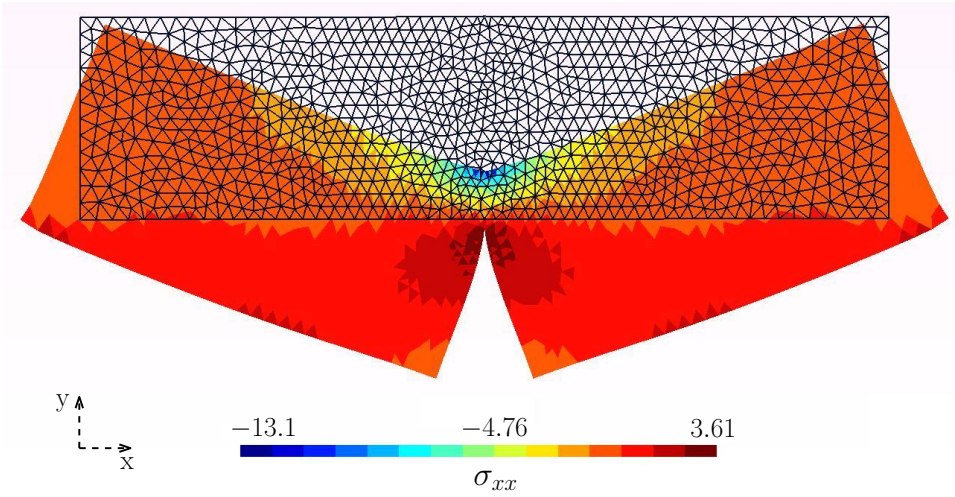

Figure 6.2: Undeformed mesh and deformed shape of the beam with a crack

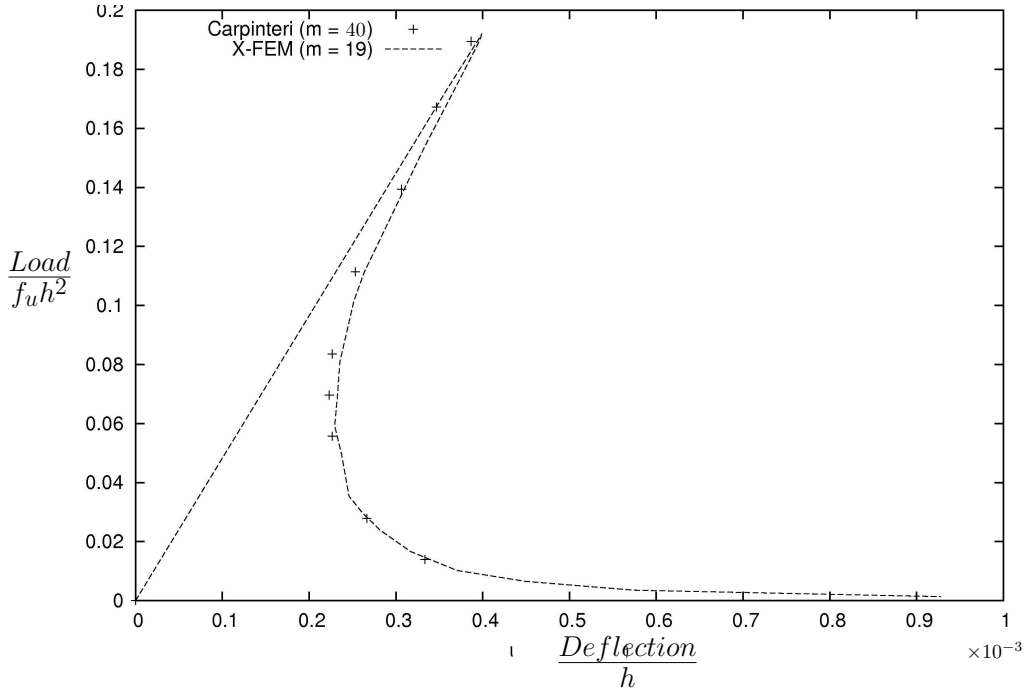

(a) $G_f = 5\,Nm^{-1}$

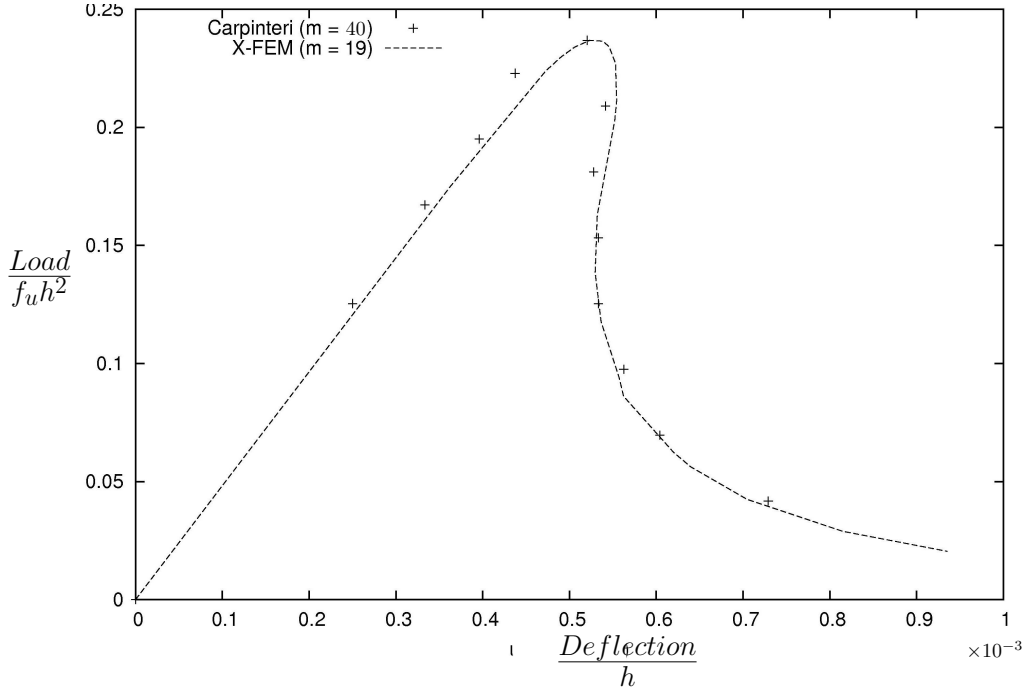

(b) $G_f = 50\,Nm^{-1}$

Figure 6.3: Non-dimensional load-deflection curves for three point bending test

```
# Table of results :
# General information of the problem:
# Lenth Scale(h) = 150, Load length(d) = 10, Thickness(t) = 150
# Spring_k = 106.3, Critical opn(Wc) = 0.03
# Ultimate Tensile Str(fu) = 3.19, Fracture Energy(Gf) = 0.05
# Brittleness Number(sE) = 0.0001
#-------------------------------------------------------------------------------------------------------------------------------
#     Step    Crack L.    L.Factor          Load          uc      Load/fuh2          uc/h      Residual       SIF I      Coh.L.       CMOD      Energy
#-------------------------------------------------------------------------------------------------------------------------------
          0           0           0             0           0             0             0
          0           0           0             0           0        0.1743     0.0003612
          0           0       10.72      1.608e+04    -0.07094         0.224     0.0004729     4.997e-14     4.997e-14       30.92     0.003005      0.3525
          0           0          11       1.65e+04     -0.0736        0.2299     0.0004907    -3.872e-14    -3.872e-14       36.08     0.004309      0.3658
          0           0        11.2       1.68e+04    -0.07588         0.234     0.0005059     2.748e-14     2.748e-14       41.23     0.005758      0.3771
          0           0       11.34        1.7e+04    -0.07851        0.2369     0.0005234     8.194e-14     8.194e-14       46.39     0.008035      0.3902
          0           0       11.31      1.697e+04    -0.08079        0.2365     0.0005386     1.274e-13     1.274e-13       51.54      0.01097      0.4016
          0           0       11.21      1.681e+04    -0.08186        0.2342     0.0005458     2.398e-14     2.398e-14       56.69      0.01301       0.407
          0           0       10.87       1.63e+04    -0.08296        0.2271     0.0005531     1.949e-14     1.949e-14       61.85       0.0166      0.4126
          0           0       10.11      1.517e+04    -0.08314        0.2113     0.0005543    -1.249e-16    -1.249e-16          67      0.02182      0.4136
          0           0       9.716      1.457e+04    -0.08285        0.2031     0.0005523     -7.795e-14    -7.795e-14       72.16      0.02409      0.4122
          1           0        8.24      1.236e+04     -0.0805        0.1722     0.0005367     -4.997e-14    -4.997e-14       77.31      0.03097      0.4008
          2          10       7.794      1.169e+04     -0.0798        0.1629      0.000532     -5.147e-14    -5.147e-14       71.46       0.0328      0.3974
          3          20       6.631           9946    -0.07944        0.1386     0.0005296      1.999e-15     1.999e-15        67.7      0.03838      0.3958
          4          30       5.634           8451    -0.08047        0.1177     0.0005364      2.998e-14     2.998e-14       64.67      0.04411      0.4011
          5          40       4.493           6740    -0.08359        0.0939     0.0005573      3.248e-14     3.248e-14       62.41      0.05239      0.4169
          6          50       4.122           6184    -0.08434       0.08615     0.0005623      2.948e-14     2.948e-14       56.53      0.05488      0.4208
          7          60       2.983           4474    -0.09302       0.06234     0.0006201      1.449e-14     1.449e-14       56.53      0.06861      0.4643
          8          70        2.69           4035    -0.09597       0.05621     0.0006398     -2.848e-14    -2.848e-14       49.75      0.07293      0.4791
          9          80       2.034           3050     -0.1057        0.0425     0.0007045     -1.569e-13    -1.569e-13       46.33       0.0858      0.5276
         10          90       1.384           2075     -0.1222       0.02892     0.0008146      4.747e-14     4.747e-14       41.98       0.1057      0.6102
         11         100      0.9777           1466     -0.1403       0.02043     0.0009354      4.597e-14     4.597e-14       38.19       0.1263      0.7006
```

Figure 6.4: Output table for three point bending test with $G_f = 50\,Nm^{-1} (s_E = 1e^{-4})$

In the table shown in figure 6.4, *Load* and u_c are the critical load and the vertical displacement of point of load application at the unset of real crack propagation respectively. The terms *Crack L.* and *Coh L.* are the real crack length and the length of cohesive zone respectively. The term *Residual* is the absolute value of the difference between value of crack propagation criterion with its critical value needed for fictitious crack propagation (residual should be zero in the case where the crack propagation criterion is fulfilled). It is observed from this table that the values of residual are very close to zero. The term *SIF-I* is the value of K_I at mathematical crack tip. The term *CMOD* is *Crack Mouth Opening* which is the opening of the crack at the point where it initiates from (middle of the lower edge of the beam). The term *Energy* is the elastic stress-strain energy input in the system provided by the load until real crack propagation.

In algorithm 2, the first data obtained by the code for cohesive crack model are the ones in step 1 in the table shown in figure 6.4. These data correspond to crack propagation unset for a body with no initial real crack and with maximum cohesive zone length. The zero steps data correspond to the cases where the cohesive zone is evolving but it has not reached its maximum length. Such data are obtained by solving the problem with cohesive zone lengths smaller than the maximum one and are obtained automatically by the code during the solution procedure.

6.2.3 Mesh size and numerical accuracy

The computations for mesh size optimization of the problem are done on a 2-D mesh of first order triangular elements. For these computations Algorithm 2 together with SIF-I criterion for crack propagation is used. Figure 6.5 shows part of the mesh around fictitious crack tip and also 1-D segments in the cohesive zone. It is observed from this figure that the mesh does not need to conform to the geometry of the crack. Note that maximum size of 1-D segments can be defined by the user and is independent of domain mesh size.

Carpinteri and *Colombo* [16] have done a numerical study in order to investigate the effect of mesh size on numerical accuracy for different brittleness numbers (s_E), from which they proposed the following equation for the lower bound of the brittleness number for materials with $\epsilon_u = 8.74e^{-5}$.

$$s_E = \frac{w_c}{tmh_m} \approx \frac{80}{m} \times 10^{-5} \tag{6.3}$$

where m is number of elements on the height of the beam (h) in the center of the beam span and h_m is the mesh size around crack tip. This equation can be written in the following form:

$$h_m < 600 w_c \tag{6.4}$$

(6.3) can also be written in the following form:

$$N_c \equiv \frac{l_{ch}}{h_m} \geq 10 \tag{6.5}$$

In this equation l_{ch} is the characteristic length of the material and is given by

$$l_{ch} = \frac{G_f E^*}{f_u^2} \tag{6.6}$$

where $G_f$is the fracture energy and E^* is the same as in (2.4). It is clear from the definition that characteristic length of the material is a material property and is of order of cohesive zone length of the material (see (2.15)). (6.5) has been used by *N. Moës* and *T. Belytschko* [37] to investigate the effect of mesh size on accuracy of numerical results.

In the present study, (6.5) is used to investigate the effect of mesh size on quality of the results. Figure 6.6 shows the non-dimensional load-deflection curves for different values of N_c with a constant mesh size (m = 17) and with 1-D segments having the same size as the mesh (not divided). It is observed from figure 6.6 that as the material becomes more brittle, a finer mesh is required to obtain acceptable results. The results are acceptable for values of N_c bigger than the threshold $N_c = 6$.

Figure 6.7 shows the dimensionless load-deflection curves for $s_E = 2e^{-5}$ (the same characteristic length for all curves) and different mesh sizes with 1-D segments having the same size as the mesh (not divided). It is observed from figure

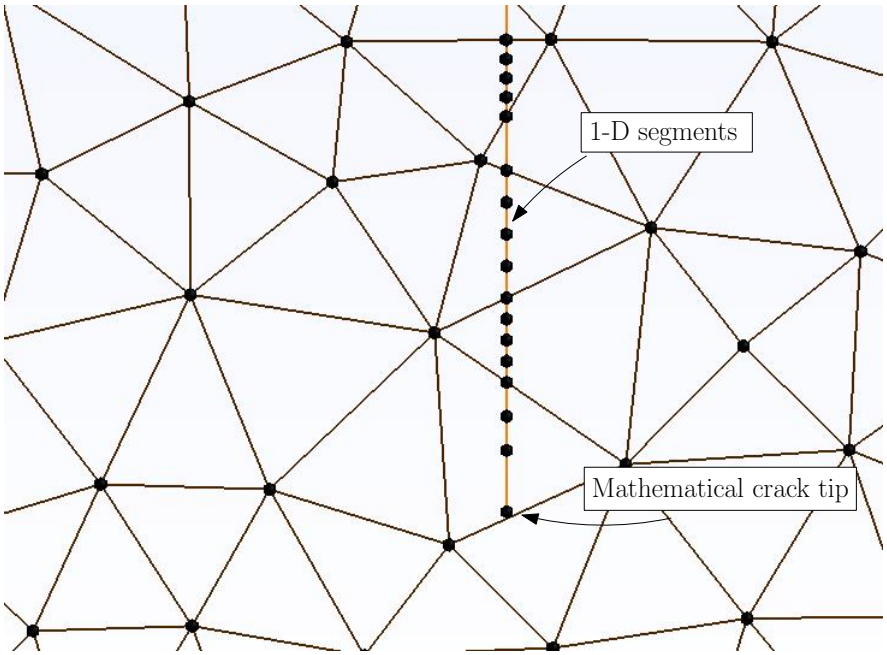

Figure 6.5: Mesh for the domain and cohesive zone

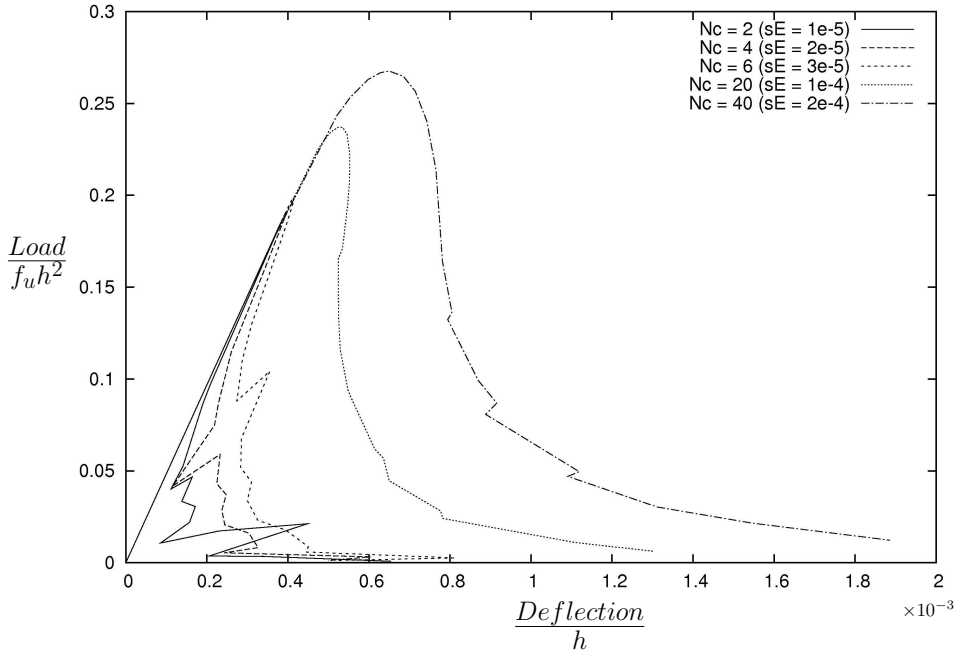

Figure 6.6: Non-dimensional load-deflection curves for different values of Nc and a constant mesh size (m = 17) with the length of 1-D segments not divided

6.7 that for $N_c = 6$ (i.e. m = 26) the results are stable. This result is the same as what obtained from figure 6.6.

In order to investigate the effect of size of 1-D segments on the numerical results, the same computations are done with length of 1-D segments divided by 2 and 3. Figure 6.8 shows the non-dimensional load-deflection curves for a constant brittleness number $s_E = 2e^{-5}$ and constant mesh size (m = 8) but with different sizes of 1-D segments (not divided, divided by 2 and 3).

It is observed from figure 6.8 that the size of 1-D segments has a big effect on the accuracy of numerical results and for smaller segments (i.e. div = 3) the results are without oscillations and are acceptable. The reason is that the ductile to brittle behavior of the material is mainly due to values of stress in cohesive zone which are applied on 1-D segments. Smaller segments can increase the accuracy of integrations over Gauss points in 1-D segments. Furthermore a good approximation of the cohesive zone length during iterations over 1-D segments depends so much on the size of these elements.

Figure 6.9 shows the non-dimensional load-deflection curves for different values of N_c and a constant mesh size (m = 17) with the length of 1-D segments divided by three. It is observed from this figure that more brittle behaviors of the beam can be captured with 1-D segments divided by three compared to the case of 1-D segments not divided. The value of $N_c = 2$ is then the threshold in this case that is one third of the case of 1-D segments not divided.

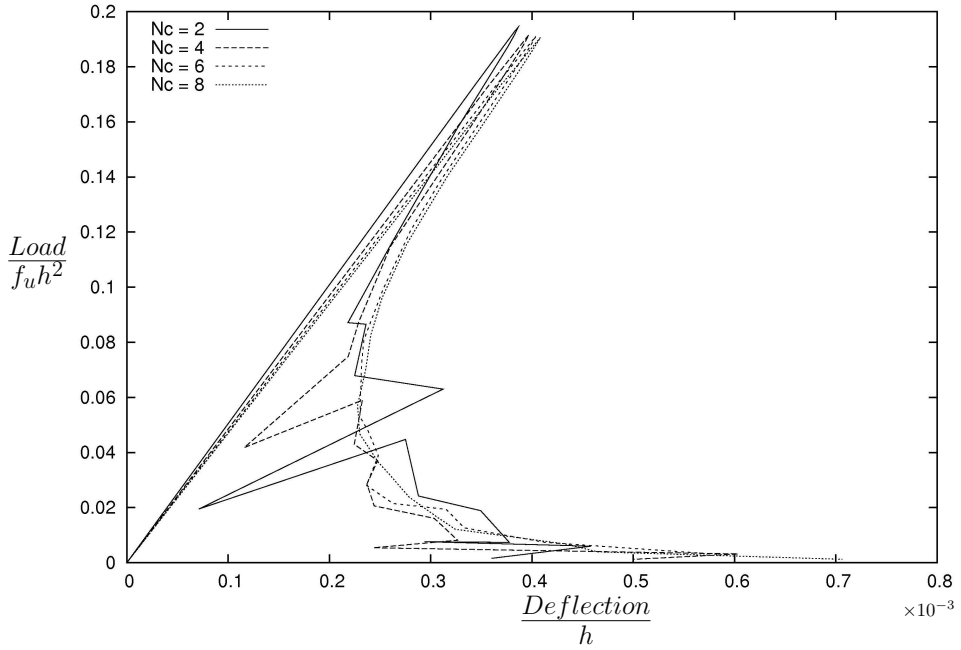

Figure 6.7: Non-dimensional load-deflection curves for a material with constant brittleness number ($s_E = 2e^{-5}$) and different mesh sizes and with the length of 1-D segments not divided

Figure 6.10 shows the dimensionless load-deflection curves for $s_E = 2e^{-5}$ (the same characteristic length) and different mesh sizes with the length of 1-D segments divided by three. It is observed from this figure that for $N_c = 2$ (i.e. m = 8) the results are stable. This results is the same as what obtained from figure 6.9.

According to results mentioned above the following conclusions can be made:

1. Decreasing the size of 1-D segments increases the numerical accuracy so much. Since the number of 1-D segments are not so many, the decrease in the size of 1-D segments does not increases so much the computational costs.

2. The threshold for value of N_c to have acceptable results for the case of 1-D segments not divided is $N_c = 6$ and for the case of 1-D segments divided by three is $N_c = 2$ which compared to the threshold obtained by *Carpinteri* and *Colombo* [16] ($N_c = 10$) using FEM, shows the efficiency in numerical accuracy of X-FEM used in this study.

6.2.4 Effect of different algorithms on the results

Several computations have been done using algorithms 1, 2 and 3 mentioned in section 5.3.5. It was observed that algorithms 1 and 2 give the same results with

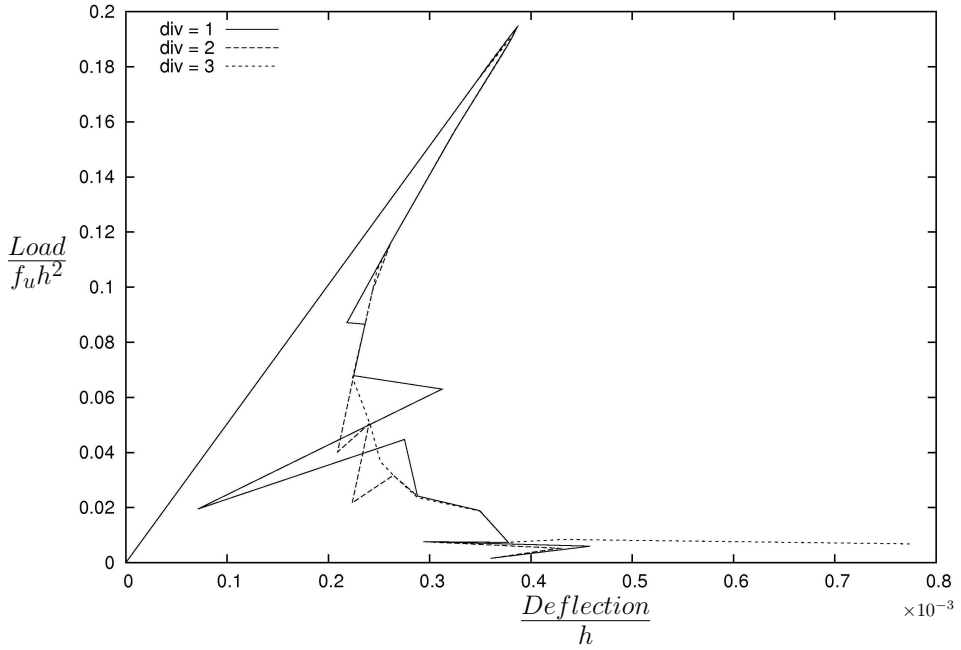

Figure 6.8: Non-dimensional load-deflection curves for constant brittleness number $s_E = 2e^{-5}$ and constant mesh size (m = 8) but with different sizes of 1-D segments

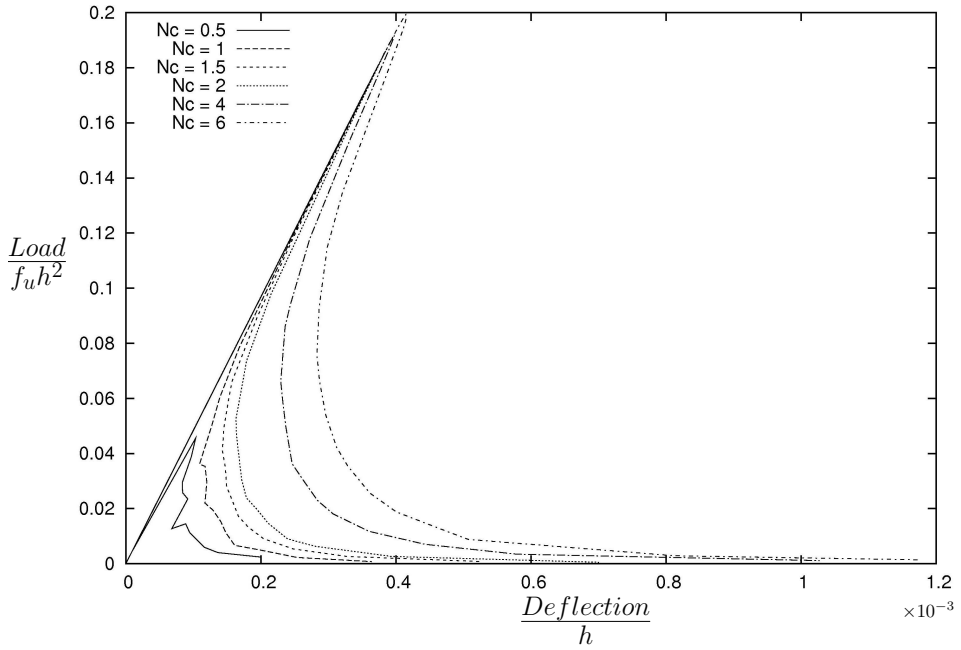

Figure 6.9: Non-dimensional load-deflection curves for different values of Nc and a constant mesh size (m = 17) with the length of 1-D segments divided by three

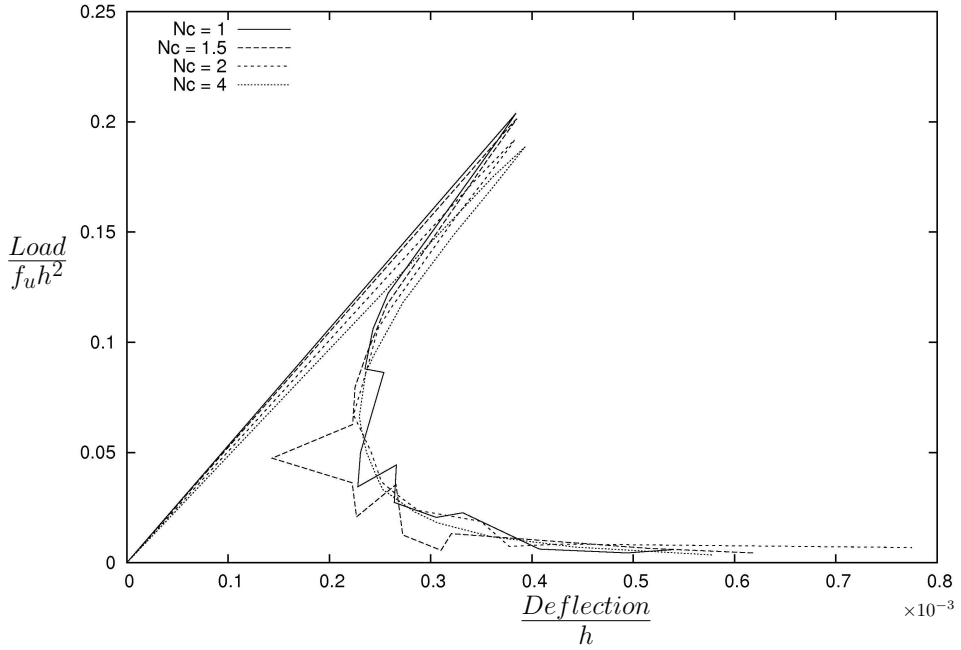

Figure 6.10: Non-dimensional load-deflection curves for a material with constant brittleness number $s_E = 2e^{-5}$ and different mesh sizes and with length of 1-D segments divided by three

the same numerical accuracy and computational costs for both crack propagation criteria. But in the code developed by the author of this thesis for numerical computations, the results from algorithm 3 did not converge for both crack propagation criteria and in most cases algorithm 3 failed to obtain reasonable results for a reasonable fine mesh.

The reason why algorithm 3 fails is maybe the fact that in this algorithm during iterations on 1-D segments, the proper size of the cohesive zone is determined for a load factor which is not the one that fulfills the crack propagation criterion at mathematical crack tip and hence is not physical. This fact makes the nonlinear problem quite sensitive to the values of load factor inside the iteration on the load factor. But in algorithm 1 and 2 the value of the load factor which fulfills the crack propagation criterion at mathematical crack tip (a physical value) is first obtained exactly in three iterations thanks to the linearity of the problem for a constant cohesive zone length, and then the proper size of cohesive zone is obtained for this load factor which seems more physical. This fact makes algorithms 1 and 2 more robust and accurate compared to algorithm 3.

Note that in the code developed by *N. Moës* and *T. Belytschko* in [37], they succeeded to obtain reasonable results using algorithm 3. In the rest of this study the computations are done using algorithm 2.

6.2.5 Effect of crack propagation criteria on the results

In order to see the effect of different crack propagation criteria on the accuracy of the results, several computations are done using algorithm 2 (the results are the same for algorithm 1) with SIF-I and stress crack propagation criteria.

Figure 6.11 shows the non-dimensional load-deflection curves for $s_E = 2e^{-5}$ and different mesh sizes and with length of 1-D segments divided by three for both criteria. Note that in this figure the results for a very fine mesh ($N_c = 17$) are also presented as a reference for accurate results.

It is observed from figure 6.11 that the results have the same behavior for both criteria regarding the accuracy for different values of N_c and that the threshold for acceptable results for stress criterion is the same as SIF-I criterion and is $N_c = 2$. But regarding the computational costs, since the computational costs for evaluating K_I in SIF-I criterion is much more than evaluating stress value at the mathematical crack tip in stress criterion, the overall computational cost for algorithms with SIF-I criterion is more than computational cost for algorithms with stress criterion.

The rest of the computations in this study are done using algorithm 2 with SIF-I criteria. In order to have more accuracy for the results, a mesh of second order 2D triangles with $m = 19$ and with length of 1-D segments divided by three is used.

6.2.6 Effect of brittleness number

In order to investigate the ductile to brittle change of behavior of the beam, several computations are done for different values of brittleness number (s_E). Figure 6.12 shows the non-dimensional load-deflection curves. Note that the change in values of brittleness number is done by varying G_f while keeping h and f_u constant ($h = 150\,mm$ and $f_u = 3.19\,MPa$). It is observed from this figure that the ductile to brittle change of the behavior of the beam decreasing the brittleness number is captured using cohesive crack model.

Figure 6.13 shows the non-dimensional load-deflection curves for the cases where h is varied independently while keeping other parameters in brittleness number constant. Note that in this case in order to maintain the geometrical similarity of the beam, $\lambda = L/h$ should be kept constant. Exactly the same curves can be obtained for the cases where f_u is varied independently while keeping other parameters in brittleness number constant. Note that in this case $\epsilon_u = f_u/E$ should be kept constant.

It is observed from figure 6.12 and 6.13 that the simple variation in brittleness number s_E produces all the cases related to the independent variations in G_f, h and f_u. Not the single values of G_f, h and f_u, but their function s_E effects the ductile to brittle change of behavior of the beam. Hence a small beam or a

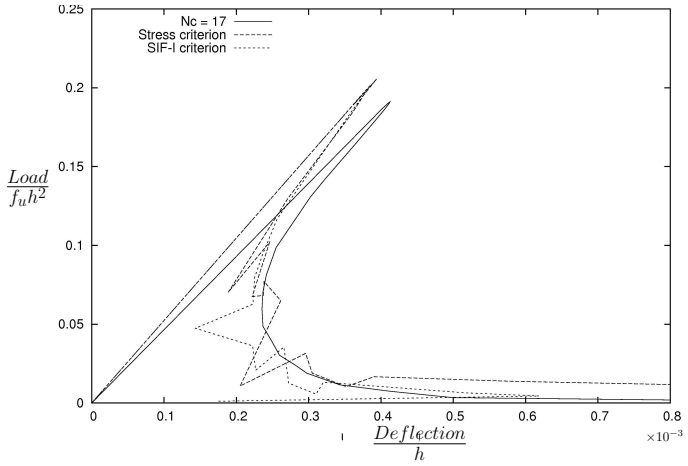

(a) Nc = 1.5

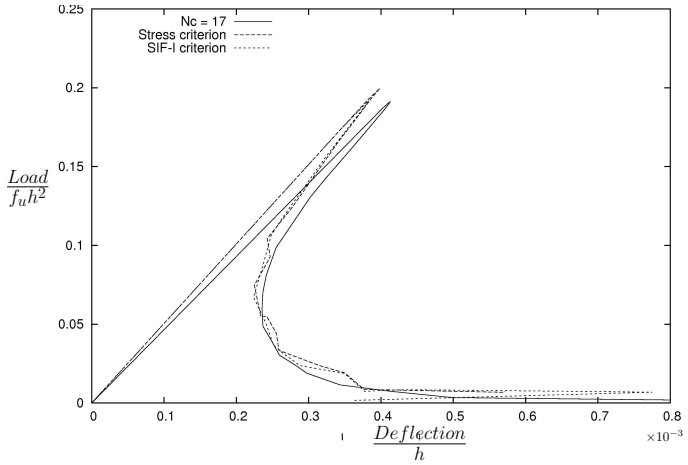

(b) Nc = 2

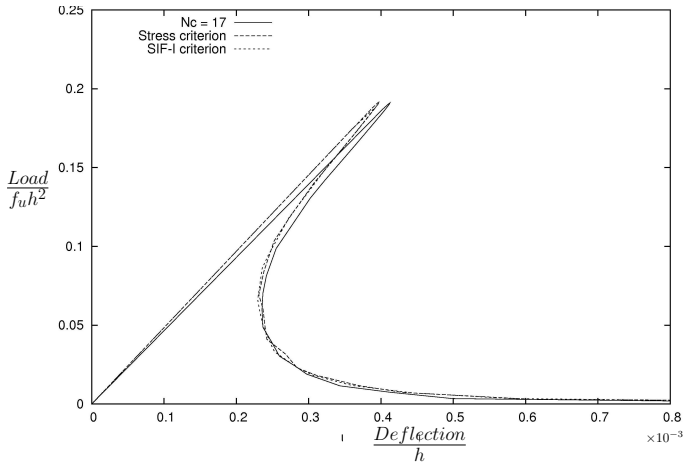

(c) Nc = 4

Figure 6.11: Non-dimensional load-deflection curves for brittleness number $s_E = 2e^{-5}$ and different mesh sizes and with length of 1-D segments divided by three (Stress criterion vs SIF-I criterion)

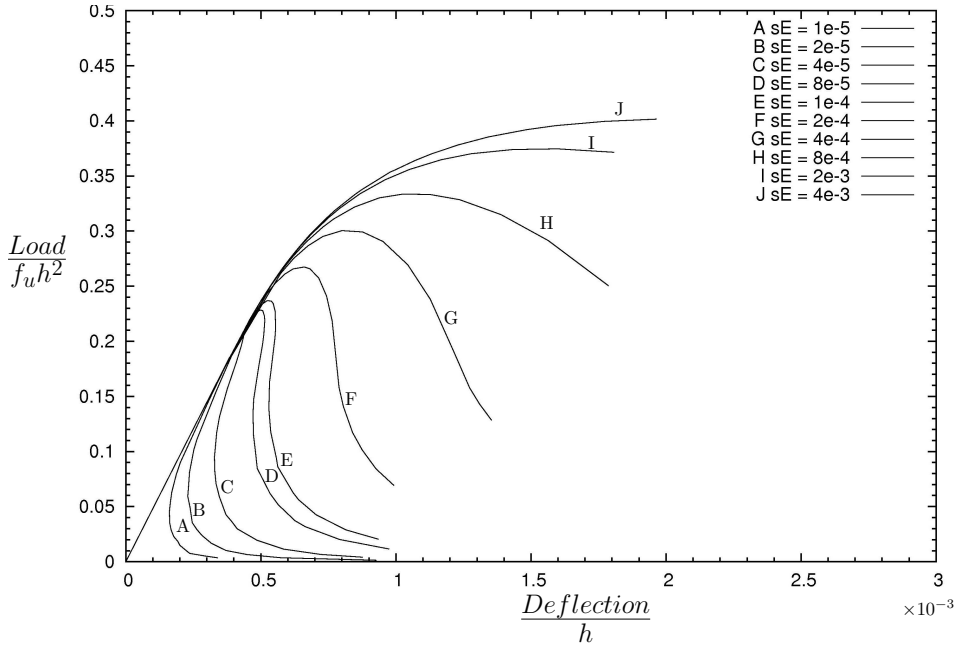

Figure 6.12: Non-dimensional load-deflection curves for different values of brittleness number for a beam with no initial crack

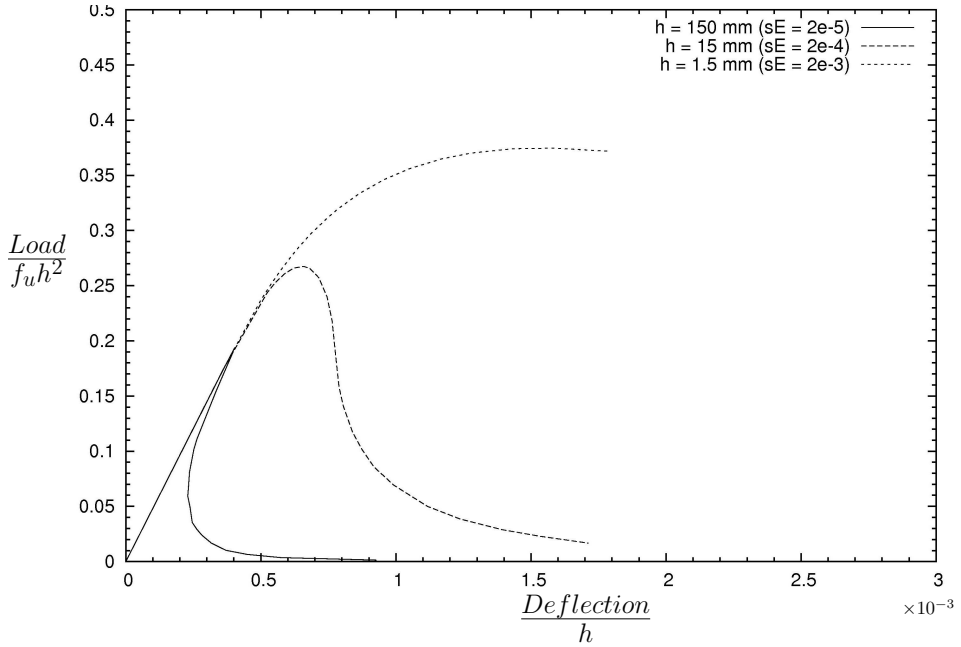

Figure 6.13: Non-dimensional load-deflection curves for different sizes of the beam for a beam with no initial crack

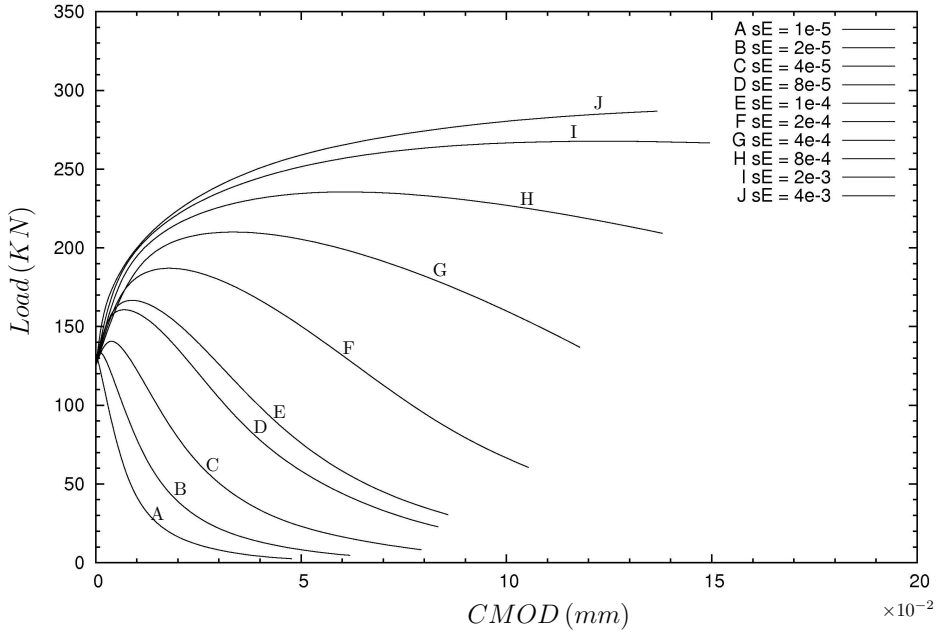

Figure 6.14: Load-CMOD curves for different values of brittleness number for a beam with no initial crack

beam made of a material with high G_f or low f_u has a ductile behavior while a large beam or a beam made of a material with low G_f or high f_u has a brittle behavior.

It is observed from figure 6.12 that snap back phenomenon happens for $s_E \leq 1e^{-4}$. Since the numerical tests are controlled by the crack length, which is monotonically increasing with time, the load-deflection data can be captured during the snap back (see section 2.1.7). As is shown in figure 6.14, crack mouth opening (CMOD) also increases monotonically during the test. Hence as mentioned in section 2.1.7, the load-deflection data can also be captured during the snap back by conducting a test in which the crack mouth opening (CMOD) is controlled.

The length of cohesive zone at maximum load is plotted against $1/s_E$ for a beam with no initial crack in figure 6.15. The change of behavior of the beam from ductile to brittle with the change in the values of s_E is again evident from this figure such that for big values of s_E the cohesive zone covers the whole hight of the beam which leads to a ductile behavior while for small values of s_E it tends to disappear and hence causing a brittle behavior.

In order to investigate the ability of LEFM to express ductile to brittle change of behavior of the beam, several computations have been done using LEFM model instead of cohesive crack model for different values of brittleness number. Figure 6.16 shows the non-dimensional load-deflection curves obtained using LEFM

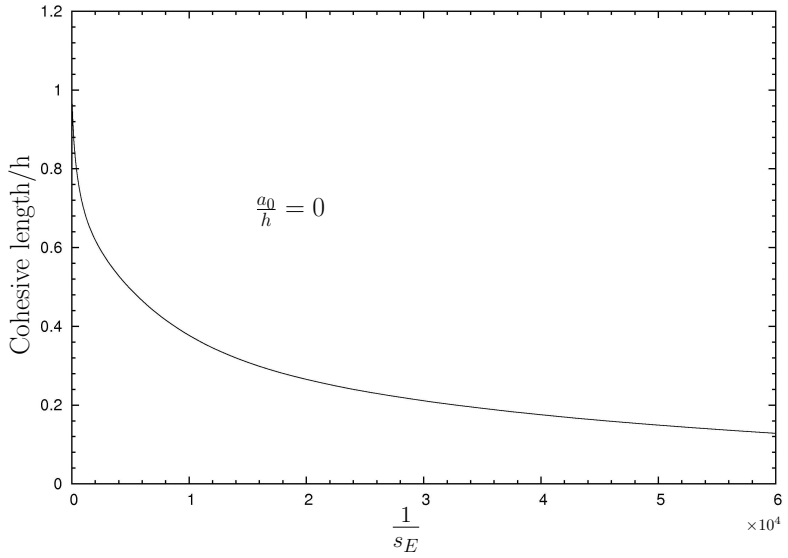

Figure 6.15: Length of cohesive zone as a function of inverse of brittleness number for three point bending test with $a_0/h = 0$

model for different values of brittleness number. It is observed from figure 6.16 that although LEFM can express the scale effects on the nominal strength of the beam (see (2.11)), since the state of stress filed in process region is not considered in this model, the behavior of the structure is brittle in all cases and LEFM is unable to express the ductile to brittle change of behavior of the beam.

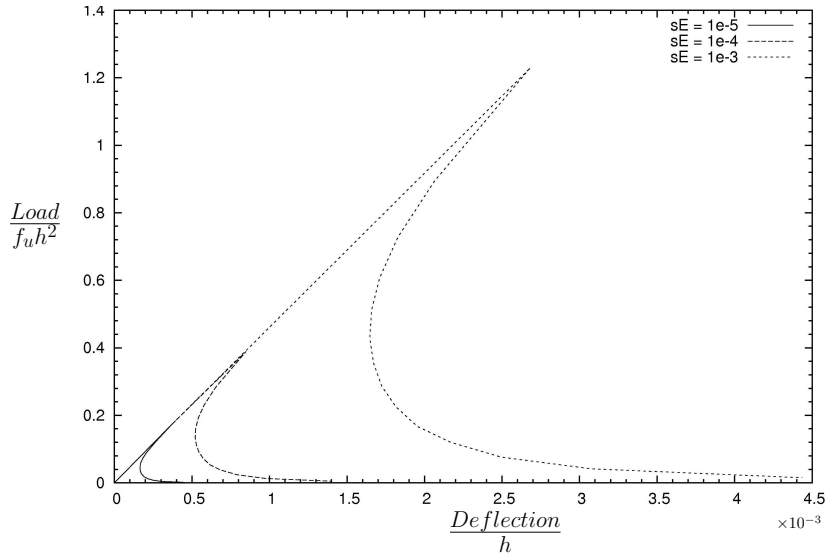

Figure 6.16: Non-dimensional load-deflection curves using LEFM model for different values of brittleness number for a beam with no initial crack

6.2.7 Effect of initial cracks

The non-dimensional load-deflection curves for different values of brittleness number for a beam with an initial crack are presented in figures 6.17, 6.18, 6.19, 6.20 and 6.21. It is observed from these figures that obviously the stiffness and maximum loading capacity of the specimen decreases by increasing the initial crack length. It is also observed that the initial crack makes the behavior of the beam more ductile than the case with no initial crack. This fact can be observed better in figure 6.21 where the beam shows a completely brittle behavior and also a snap back for the case without initial crack ($a_0/h = 0$) but the behavior changes to ductile without any snap back for the cases with $a_0/h \geq 0.3$.

It also appears from figures 6.20 and 6.21 that the non-dimensional load-deflection curves for different initial crack lengths share the same part at the end of the softening branch. This fact is due to the assumption of a damage zone collinear to the crack and concentrated on a line of zero thickness in cohesive crack model. It can be also observed from figures 6.20 and 6.21 that the real crack length for maximum load is the same as initial crack length which means that the real crack does not grow before the softening stage (decrease in the load).

The length of cohesive zone at maximum load is plotted against $1/s_E$ for a beam with different initial crack lengths in figure 6.22. Like figure 6.15 the change of behavior of the beam from ductile to brittle with the change in

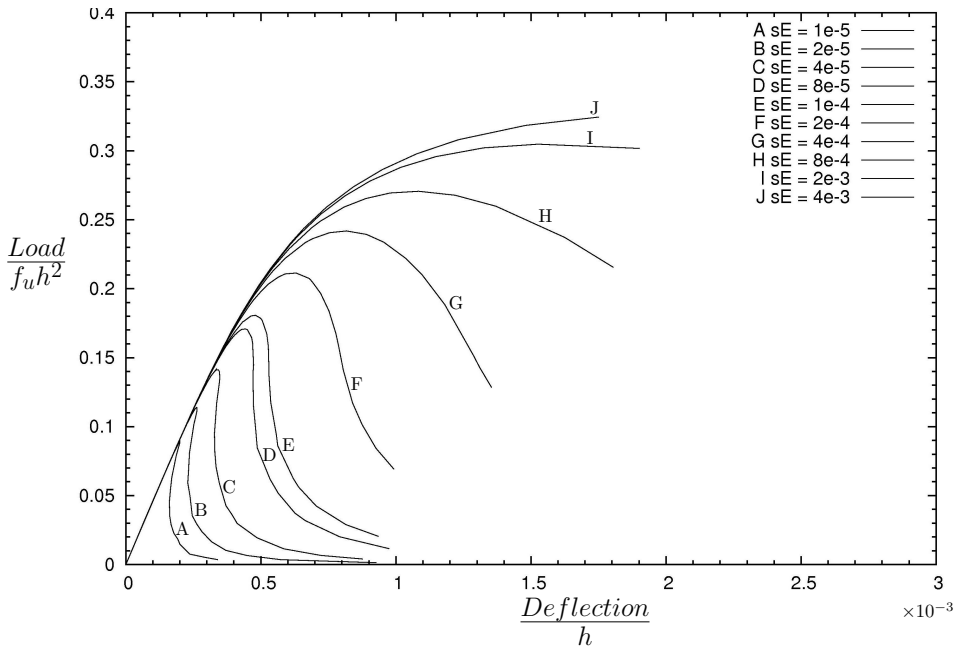

Figure 6.17: Non-dimensional load-deflection curves for different values of brittleness number for a beam with an initial crack depth of $a_0/h = 0.1$

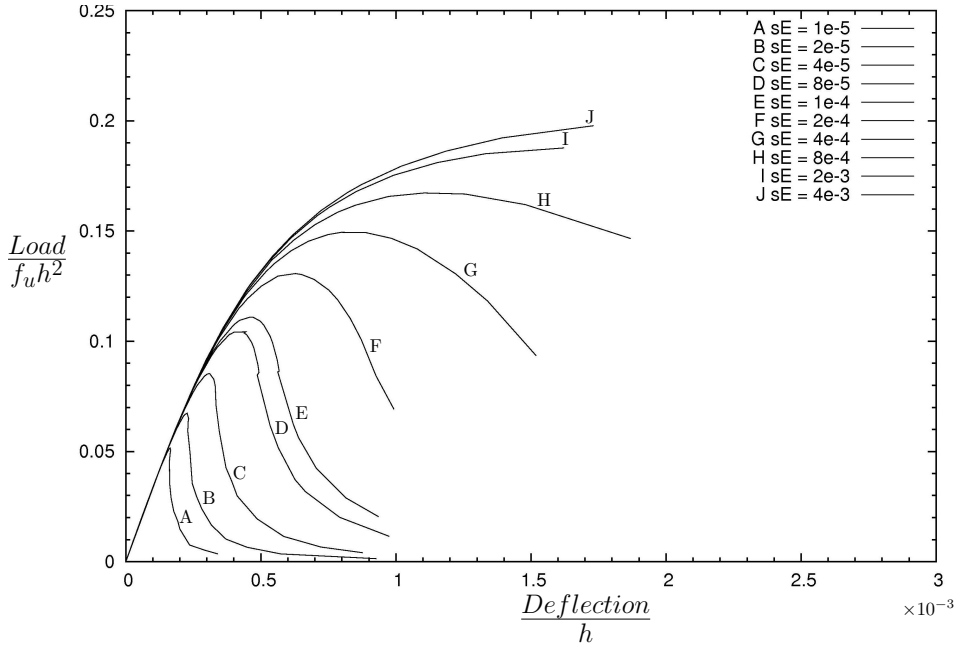

Figure 6.18: Non-dimensional load-deflection curves for different values of brittleness number for a beam with an initial crack depth of $a_0/h = 0.3$

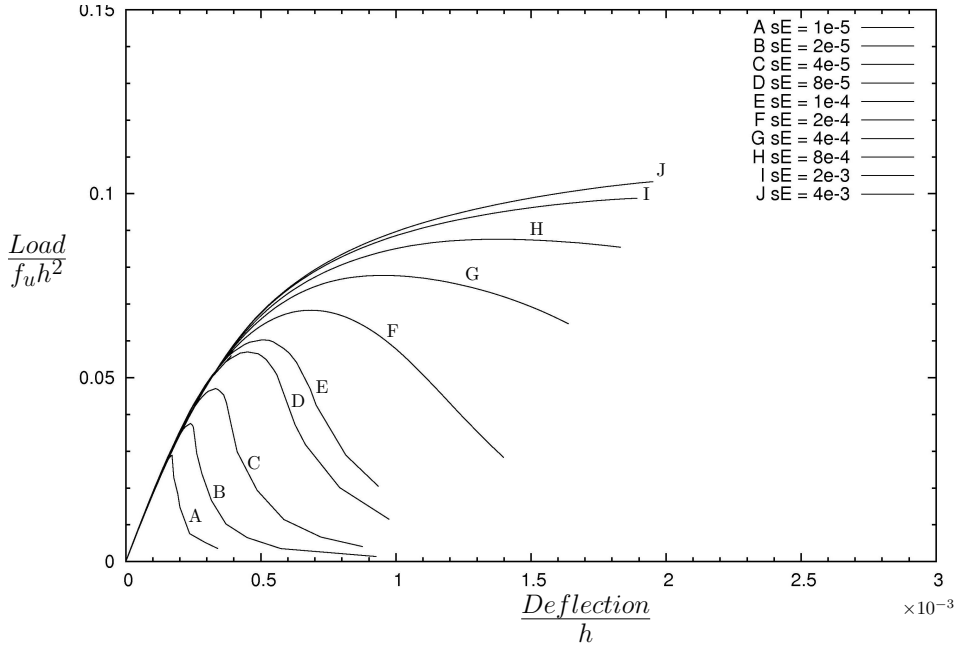

Figure 6.19: Non-dimensional load-deflection curves for different values of brittleness number for a beam with an initial crack depth of $a_0/h = 0.5$

the values of s_E can be observed from this figure. It is also observed that the length of cohesive zone for a constant value of s_E decreases for beams with longer initial crack length, but for very small values of s_E (very brittle material or a large specimen) the length of the cohesive zone converges to a value which is a material property (see section 2.1.8). This also confirms the fact that the size of cohesive zone for structures with a brittle behavior is small and independent of specimen geometry and real crack length (one of the main assumptions for LEFM).

6.2.8 Apparent and real properties

Beam without initial crack

The value of maximum load capacity for three point bending test without initial crack can be obtained analytically using an ultimate strength elastic limit analysis from the following equation:

$$P_{U.S.} = \frac{2}{3}\frac{f_u t h^2}{L} \tag{6.7}$$

In order to investigate the size effects on a beam without initial crack, the ratio of maximum load capacity (P_{Coh}) obtained from figure 6.12 to the maximum load of ultimate strength ($P_{U.S.}$) obtained from (6.7) is plotted for different values of $1/s_E$ as shown in figure 6.23. This ratio can be regarded as the ratio

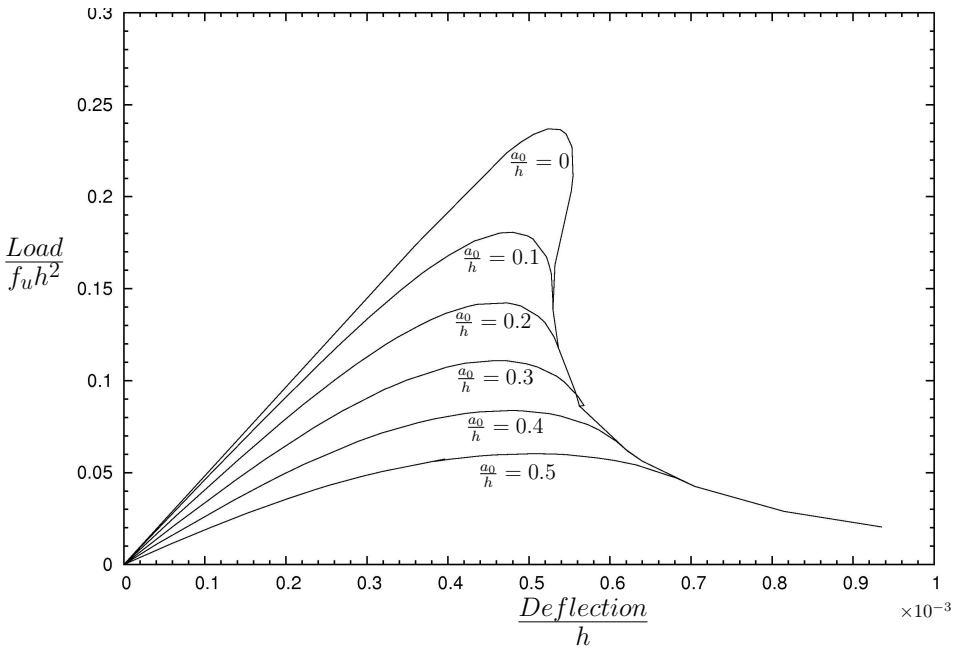

Figure 6.20: Non-dimensional load-deflection curves for $s_E = 1e^{-4}$ for a beam with different initial crack length

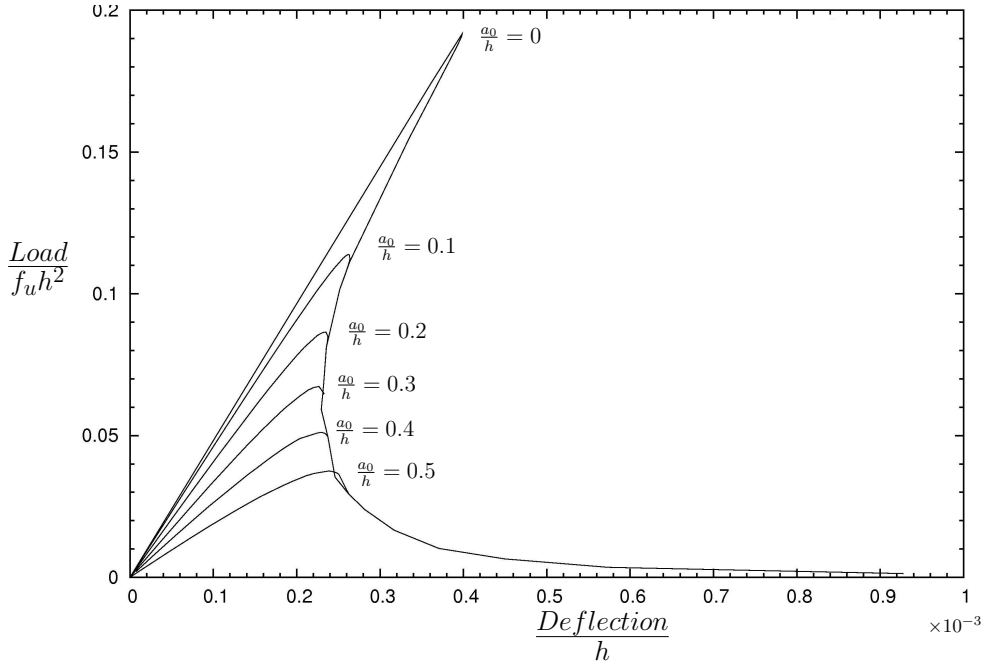

Figure 6.21: Non-dimensional load-deflection curves for $s_E = 2e^{-5}$ for a beam with different initial crack length

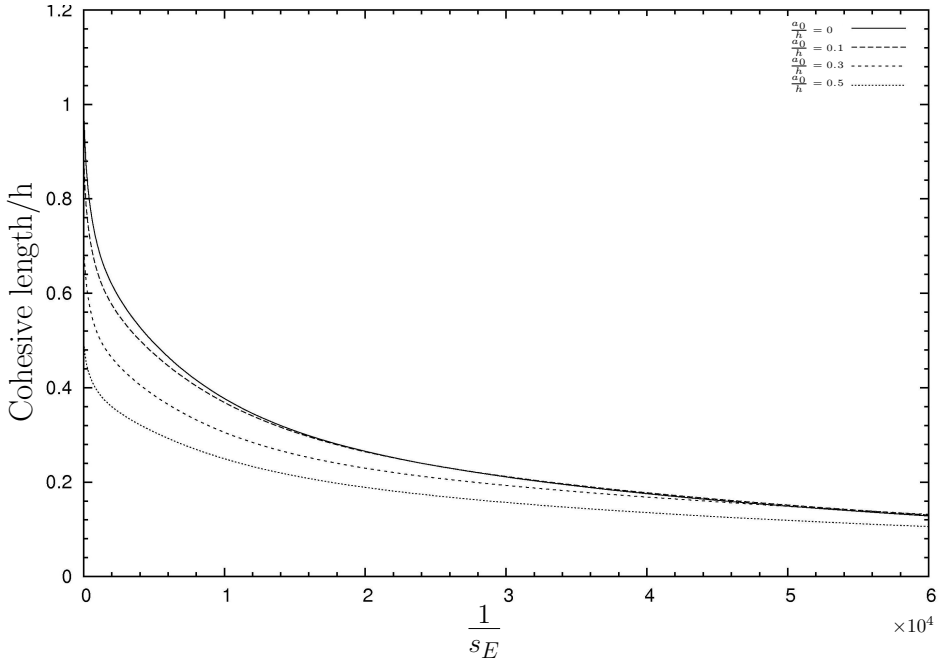

Figure 6.22: Length of cohesive zone as a function of inverse of brittleness number for three point bending test for a beam with different initial crack lengths

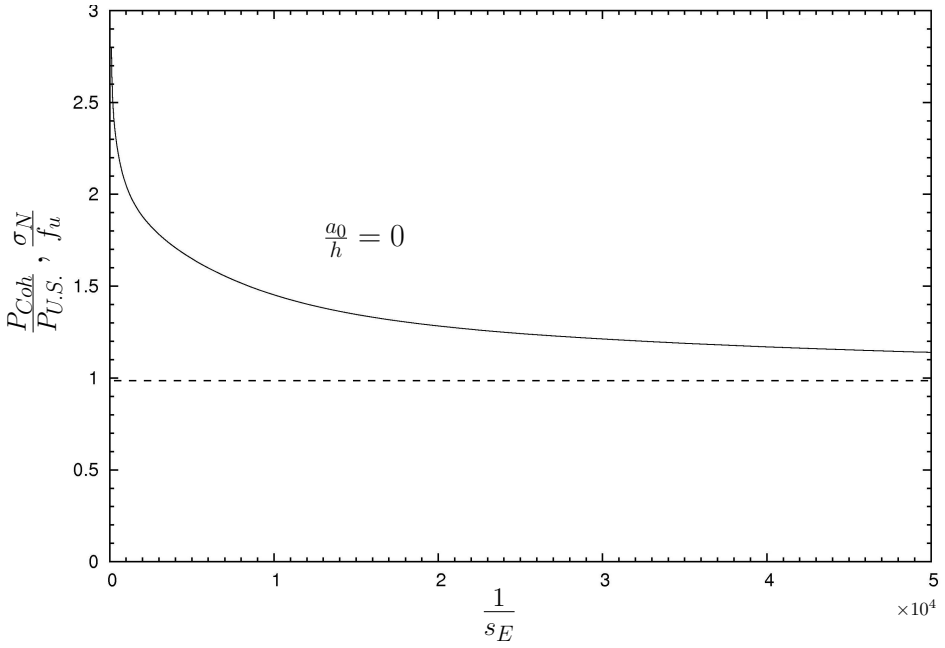

Figure 6.23: Apparent strength v.s. real strength of the material for different values of brittleness number for a beam with no initial crack

of nominal ultimate stress at failure (σ_N or apparent strength) obtained by applying (6.7) to P_{Coh} (see (2.8)), to the real ultimate strength of the material (f_u).

The following relationships can be observed from figure 6.23:

$$\lim_{s_E \to 0} \sigma_N = f_u \tag{6.8}$$

$$\lim_{s_E \to \infty} \sigma_N = 3 f_u \tag{6.9}$$

which means that the value of apparent ultimate strength of the material is more than the real ultimate strength of the material but it will tend to the real ultimate strength for small values of s_E (e.g. big specimens). From this one can conclude that with the usual laboratory specimens, an apparent strength higher than the true one is always obtained.

It is observed from figure 6.23 that $\sigma_N \to 3 f_u$ for big values of s_E. The reason is that the behavior of the material is elastic perfectly plastic in tension for big values of s_E. In such cases when the maximum load is applied to the beam a uniform stress distribution is made at the center of the beam which acts like a plastic hinge with a resistant moment (M_{max}) that is three times more than the resistant moment obtained by linear elastic stress distribution (see figure 6.24).

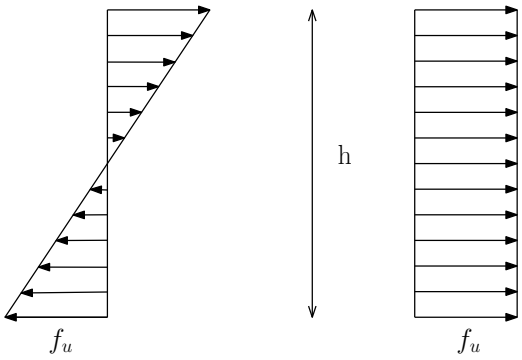

$M_u = \frac{1}{6} f_u t h^2$ $M_{max} = \frac{1}{2} f_u t h^2$

$M_{max} = 3M_u$

Figure 6.24: Elastic and elastic perfectly plastic distribution of stress in the center of the beam

Beam with an initial crack

The value of maximum load capacity (P) for three point bending test with an initial crack of length a_0 can be obtained using different approaches depending on the beam behavior. Using an LEFM approach P can be obtained analytically from the following equation:

$$P_{LEFM} = \frac{K_{Ic} t h^{3/2}}{L g(a_0/h)} \tag{6.10}$$

where K_{Ic} is the fracture toughness and can be obtained according to the following relationship (see (2.7)):

$$K_{Ic} = \sqrt{G_f E^*} \tag{6.11}$$

where E^* is the same as in (2.4). In (6.10), $g(a_0/h)$ is a function which represents the geometry of structure or specimen (see (2.15)) and for three point bending test is approximated by the following equation [1]:

$$\begin{aligned} g\Big(\frac{a_0}{h}\Big) = 2.9\Big(\frac{a_0}{h}\Big)^{1/2} - 4.6\Big(\frac{a_0}{h}\Big)^{3/2} + 21.8\Big(\frac{a_0}{h}\Big)^{5/2} \\ - 37.6\Big(\frac{a_0}{h}\Big)^{7/2} + 38.7\Big(\frac{a_0}{h}\Big)^{9/2} \end{aligned} \tag{6.12}$$

Note that the values of P_{LEFM} can also be obtained from numerical computations using LEFM model as is done for the present study.

Using a simple ultimate strength limit analysis on the center-line of the beam with assumption of butterfly stress variation through the ligament, P can be obtained analytically from the following equation:

$$P_{U.S.} = \frac{2}{3} \frac{f_u t (h - a_0)^2}{L} \tag{6.13}$$

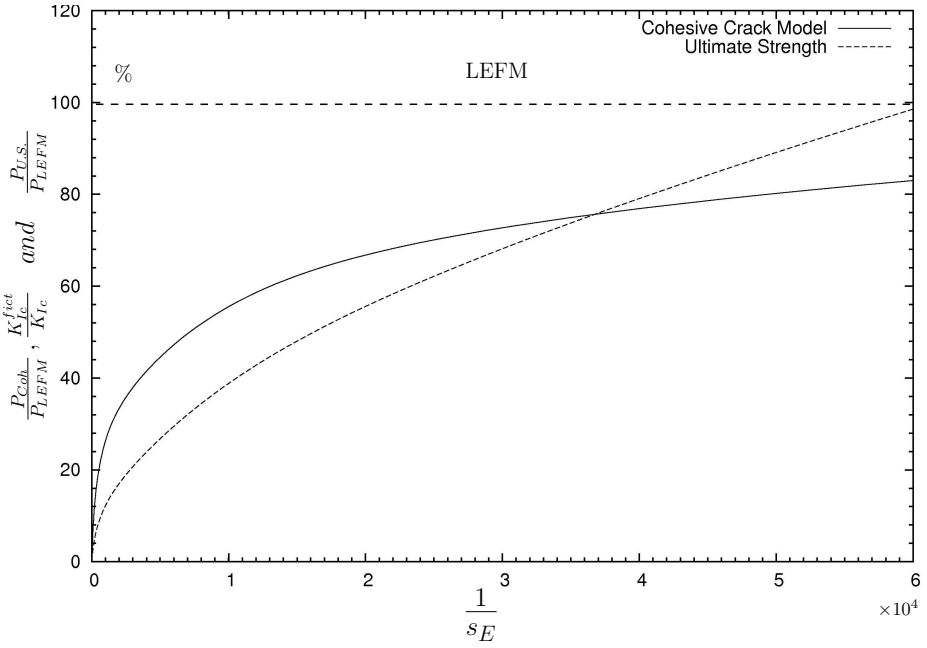

Figure 6.25: Fictitious fracture toughness v.s. real fracture toughness of the material for different values of brittleness number for a beam with an initial crack depth of $a_0/h = 0.5$

Using cohesive crack model approach, $P(P_{Coh}$ in this case) is the maximum load obtained from non-dimensional load-deflection curves presented in figures 6.17, 6.18 and 6.19.

In order to investigate the size effects on a beam with an initial crack, the values of ratios $P_{U.S.}/P_{LEFM}$ and P_{Coh}/P_{LEFM} for a beam with a crack depth of $a_0/h = 0.5$ are presented as a function of $1/s_E$ in figure 6.25. The ratio P_{Coh}/P_{LEFM} can be regarded as the ratio of fictitious fracture toughness (K_{Ic}^{fict} or apparent fracture toughness) obtained by applying (6.10) to P_{Coh}, to the real fracture toughness of the material (K_{Ic}).

It is observed from figure 6.25 that the value of apparent fracture toughness of the material is less than the real fracture toughness of the material but it will tend to the real fracture toughness for small values of s_E (e.g. big specimens). From this one can conclude that with the usual laboratory specimens, an apparent fracture toughness less than the true one is always obtained.

It is also observed from figure 6.25 that the values of $P_{U.S.}$ are less than values of P_{LEFM} and P_{Coh} for big values of s_E which confirms the fact that for a ductile material or a small beam the failure will be governed by ultimate strength. But for intermediate values of s_E the values of P_{Coh} are less than values of P_{LEFM} and $P_{U.S}$ which confirms the fact that for a quasi brittle material or a medium beam the failure will be governed by cohesive crack model (nonlinear fracture

mechanics). Finally it is observed that for small values of s_E which is the case for a brittle material or a large beam, the values of P_{Coh} tend to the values of P_{LEFM} which means that in these cases the failure will be governed by LEFM. All these observations are in agreement with Bažant's size effect law (see (2.13) and figure 2.4).

Chapter 7

Conclusions

7.1 Conclusions

The conclusions of the present study can be categorized into two groups. The first group includes the conclusions on the numerical method used to solve the cohesive crack model. The second group includes the conclusions on behavior of structure modeled by the cohesive crack model according to the numerical results obtained from the computations.

According to numerical study performed on the efficiency of X-FEM we can conclude that:

1. Using X-FEM the mesh does not need to conform to the geometry of the problem thanks to the discontinues enrichment functions used in X-FEM. Therefore there is no need for remeshing during crack propagation procedure and the same mesh can be used for all cracks.

2. X-FEM is more efficient with respect to the numerical accuracy compared to classical FEM thanks to the enrichment functions used at the crack tip that can include the a priori known behavior of the problem in numerical computations.

3. The fact that the size of 1-D segments used as the mesh for cohesive zone can be independent of the global mesh, makes it possible to increase the accuracy of the results so much without any large increase in computational costs, using small enough 1-D segments while keeping the size of the global mesh constant.

4. Using algorithms 1 and 2, proposed in this study, makes it possible to obtain numerical results with the same accuracy, using SIF-I or stress criterion.

According the results obtained from numerical computations we can conclude that:

1. Unlike LEFM, Cohesive crack model is able to express ductile to brittle change of behavior of the structure, thanks to the fact that the state of the stress field in the process zone of the crack is taken into account in this model.

2. The ductile to brittle change of behavior of the structure is not depending on the single values of fracture energy, ultimate tensile strength and structure size but on their function called brittleness number. Simple variations in this number can produce all the cases related to the variation of fracture energy, ultimate tensile strength and structure size.

3. The snap back phenomenon in brittle materials can be captured with cohesive crack model using a test in which a parameter that increases with the time, like crack length or crack mouth opening, is controlled.

4. The presence of initial cracks in the structure results in a more ductile behavior of the structure.

5. Cohesive crack model can express the size effects for three point bending test properly. The effect of scale of the beam on evaluation of ultimate tensile strength and fracture toughness of the material can be modeled using cohesive crack model.

7.2 Achievements and knowledge contribution

During my master thesis I tried to gain detailed knowledge and to study the state of the art on linear and nonlinear fracture mechanics and their ability to express the behavior of quasi brittle materials. Specifically I studied cohesive crack model as the most simple model for nonlinear fracture mechanics. I also gained a detailed knowledge and the state of the art on numerical methods used to treat linear and nonlinear crack propagation problems and more specifically on Extended Finite Element Method and level set techniques .

I developed a robust C++ routine that can include cohesive crack propagation in Xfem and Xcrack C++ libraries developed in *Institut de Recherche en Génie Civil et Méchanique (GeM)*(Institute of research on civil and mechanical engineering) at *Ecole Centrale de Nantes (ECN)*. During this phase of my thesis study, I devoted so much time to learn advanced C++ language to understand the algorithms used in Xfem and Xcrack C++ libraries and to develop my own code. I tried to code different algorithms and to compare their robustness. I devoted so much time to remove the bugs in my code and to make it as user friendly as possible regarding input parameters and output results and tables.

Finally I tried to model three point bending test as a bench test with my code and to investigate the ability of cohesive crack model to express the behavior of quasi brittle materials.

7.3 Future works

The following items can be regarded as the extension of the present work in the future:

1. Implementation of a code which includes cohesive crack model for nonlinear crack propagation in 2-D and 3-D mixed mode problems.

2. Investigation on the efficiency of cohesive crack model for problems with high stress gradient like unidirectional tensile tests.

3. Investigation on the effect of the terms related to cohesive crack model in discretized variational formulation, on condition of the resulting stiffness matrix and finding the most efficient solver to solve the resulting system of equation.

4. Development of different approaches to include cohesive crack model in the main variational formulation of the problem resulting a better conditioned stiffness matrix.

Bibliography

[1] Standard method of test for plain strain fracture toughness of metallic materials. Technical Report E399-74, ASTM. [cited at p. 56]

[2] GI. Barenblatt. The formation of equilibrium cracks during brittle fracture: general ideas and hypotheses. *J Appl Math Mech*, 23:622–36, 1959. [cited at p. 15]

[3] GI. Barenblatt. The mathematical theory of equilibrium cracks in brittle fracture. *Adv Appl Mech*, 7:55–129, 1962. [cited at p. 15]

[4] Z.P. Bažant. Iutam prager symposium on mechanics of geomaterials: Rocks, concretes, soils. pages 281–316, Northwestern University, Evanston, IL., Sept 1983. [cited at p. 13]

[5] Z.P. Bažant. *Journal of Engineering Mechanics ASCE 110*, No. 4:518–535, 1984. [cited at p. 12, 13]

[6] Z.P. Bažant. Proceedings us-japan seminar on finite element analysis of reinforced concrete structures. pages 121–150, New York, 1986. American Society of Civil Engineers. [cited at p. 13]

[7] Z.P. Bažant. Sem/rilem international conference on fracture of concrete and rock. pages 390–402. Society for Experimental Mechanics, 1987. [cited at p. 13]

[8] Z.P. Bažant and M.T. Kazemi. Determination of fracture energy, process zone length and brittleness number from size effect with application to rock and concrete. *International Journal of Fracture*, 44:111–131, 1990. [cited at p. 13, 14]

[9] Z.P. Bažant and M.T. Kazemi. Size effect in fracture of ceramics and its use to determine fracture energy and effective process zone length. *J. Am. Ceram. Soc*, 73:1841–53, 1990. [cited at p. 13, 14]

[10] T. Belytschko and T. Black. Elastic crack growth in finite elements with minimal remeshing. *Int. J. Numer Meth Engng*, 45(5):601–20, 1999. [cited at p. 20]

[11] T. Belytschko, D. Organ, and C. Gerlach. Element-free galerkin methods for dynamic fracture in concrete. *Computer Methods in Applied Mechanics and Engineering*, 187:385–99, 2000. [cited at p. 25]

[12] K. Bertram Broberg. *Cracks and Fracture*. ACADEMIC PRESS, 1999. [cited at p. 8, 9, 11]

[13] G.T. Camacho and M. Ortiz. Computational modeling of impact damage in brittle materials. *J Solids Structs*, 33:2899–938, 1996. [cited at p. 23]

[14] A. Carpinteri. Interpretation of griffith instability as a bifurcation of the global equilibrium. in: Shah sp, editor. application f fracture mechanics to cementitious composites. pages 284–316, 1985. [cited at p. 18]

[15] A. Carpinteri. Post-peak and post-bifurcation analysis of cohesive crack propagation. *Engineering Fracture Mechanics*, 32:265–278, 1989. [cited at p. 23]

[16] A. Carpinteri and G. Colombo. Numerical analysis of catastrophic softenning behavior (snap back instability). *Computers and Structures*, 31:607–636, 1989. [cited at p. 6, 15, 23, 36, 37, 40, 43]

[17] A. Carpinteri, P. Cornetti, F. Barpi, and S. Valente. Cohesive crack model description of ductile to brittle size-scale transition: dimensional analysis vs. renormalization group theory. *Engineering Fracture Mechanics*, 70:1809–1839, 2003. [cited at p. 16, 17, 23, 83]

[18] A. Carpinteri, S. Valente, G. Ferrara, and G. Melchiorri. Is mode ii fracture energy a real material property. *Comput Struct*, 48:397–413, 1993. [cited at p. 17, 23]

[19] Z. Cen and G. Maier. Bifurications and instabilities in fracture of cohesive-softening structures: A boundary element analysis. *Fracture of Engineering Materials*, 1992. [cited at p. 25]

[20] T. Chen, B. Wang, Z. Cen, and Z. Wu. A symmetric galerkin multi-zone cboundary element method for cohesive crack growth. *Engineering Fracture Mechanics*, 63:591–609, 1999. [cited at p. 25]

[21] G.P. Cherepanov. The propagation of cracks in a continuous medium. *Journal of Applied Mathematics and Mechanics*, 1967. [cited at p. 10]

[22] DC. Drucker. Some implications of work-hardening and ideal plasticity. *Quart Appl Math*, 7:411–8, 1950. [cited at p. 12]

[23] D.S. Dugdale. Yielding of steel sheets containing slits. *J Mech Phys Solids*, 8:100–14, 1960. [cited at p. 15]

[24] E. Erdogan. Fracture mechanics. *International Journal of Solids and Structures*, 27:171–183, 2000. [cited at p. 9]

[25] A. Hillerborg, M. Modeer, and P.E. Petersson. Analysis of crack formation and crack growth in concrete by means of fracture mechanics and finite elements. *Cem Concr Res*, 6:773–82, 1976. [cited at p. 15]

[26] G. Irwin. Analysis of stresses and strains near the end of a crack traversing a plate. *Journal of Applied Mechanics*, 24:361–364, 1957. [cited at p. 9]

[27] Milan Jirásek. Comparative study on finite elements with embedded discontinuities. *Computer Methods in Applied Mechanics and Engineering*, 188:307–330, 2000. [cited at p. 24]

[28] P. Krysl and T. Belytschko. Element free galerkin method for dynamic propagation of arbitrary 3-d cracks. *International Journal for Numerical Methods in Engineering*, 44(6):767–800, 1999. [cited at p. 20]

[29] Hamid R. Lotfi and P. Benson Shing. Embedded representation of fracture in concrete with mixed finite elements. *International Journal for Numerical Methods in Engineering*, 38:1307–1325, 1995. [cited at p. 24]

[30] G. Maier. Behavior of elastic-plastic trusses with unstable bars. *J Engng Mech (ASCE)*, 92:67–91, 1966. [cited at p. 12]

[31] G. Maier. Incremental plastic analysis in the presence of large displacements and physical instabilizing effects. *Int J Solids Struct*, 7:345–72, 1971. [cited at p. 12]

[32] G. Maier, G. Novati, and Z. Cen. Symmetric galerkin boundary element method for quasi-brittle-fracture and frictional contact problems. *Computational Mechanics*, 13:74–89, 1993. [cited at p. 25]

[33] G. Maier, A. Zavelani, and JC. Dotreppe. Equilibrium branching due to flexural softening. *J Engng Mech (ASCE)*, 89:897–901, 1973. [cited at p. 12]

[34] J. M. Melenk and I. Babuška. The partition of unity finite element method: Basic theory and applications. *Comp Meth Appl Mech Engng*, 39:289–314, 1996. [cited at p. 20]

[35] N. Moës, J. Dolbow, and T. Belytschko. A finite element method for crack growth without remeshing. *Int. J. Numer Meth Engng*, 46:131–50, 1999. [cited at p. 20]

[36] N. Moës, A. Gravouil, and T. Belytschko. Non-planar 3d crack growth by the extended finite element and level sets. part i: Mechanical model. *International Journal for Numerical Methods in Engineering*, 53:2549–2568, 2001. [cited at p. 22]

[37] Nicolas Moës and Ted Belytschko. Extended finite element method for cohesive crack growth. *Engineering Fracture Mechanics*, 69:818–813, 2002. [cited at p. 15, 16, 24, 27, 30, 34, 41, 45]

[38] J. Oliver. Modelling strong discontinuities in solid mechanics via strain softening constitutive equations. part 2: Numerical simulation. *International Journal for Numerical Methods in Engineering*, 39:3601–3623, 1996. [cited at p. 24]

[39] J. Oliver, A.E. Huespe, and P.J. Sánchez. A comparative study on finite elements for capturing strong discontinuities: E-fem vs x-fem. *Computer Methods in Applied Mechanics and Engineering*, 195:4732–52, 2006. [cited at p. 23]

[40] J. Planas and M. Elices. Asymptotic analysis of a cohesive crack: 1. theoretical background. *International Journal of Fracture*, 55:153–77, 1992. [cited at p. 30]

[41] J. Planas and M. Elices. Asymptotic analysis of a cohesive crack: 2. influence of the softening curve. *International Journal of Fracture*, 64:221–237, 1993. [cited at p. 30]

[42] Timon Rabczuk and Goangseup Zi. A meshfree method based on the local partition of unity for cohesive cracks. *Comput Mech*, 39:743–60, 2007. [cited at p. 25]

[43] YR Rashid. Analysis of prestressed concrete pressure vessels. *Nucl Engng Des*, 7:334–55, 1968. [cited at p. 15]

[44] J.R. Rice. A path independent integral and the approximate analysis of strain concentration by notches and cracks. *Journal of Applied Mechanics*, 35, 1968. [cited at p. 10]

[45] A. L. Saleh and M. H. Aliabadi. Crack growth analysis in concrete using boundary element method. *Engineering Fracture Mechanics*, 51(4):533–545, 1995. [cited at p. 24, 32]

[46] A Scanlon. *Time-dependent deflection of reinforced concrete slabs PPPHHHDDDf*. PhD thesis, University of Alberta, Edmonton, Canada, 1971. [cited at p. 15]

[47] M. Stolarska, D. L. Chopp, N. Moës, and T. Belytschko. Modeling crack growth by level sets and the extended finite element method. *International Journal for Numerical Methods in Engineering*, 51(8):943–960, 2001. [cited at p. 22]

[48] X-P Xu and A. Needlman. Numerical simulations of fast crack growth in brittle solids. *Journal of Mechanics and Physics of Solids*, 42:1397–1434, 1994. [cited at p. 23]

[49] B. Yang and K. Ravi-Chandar. A single-domain dual-boundary-element formulation incorporating a cohesive zone model for elstostatic cracks. *International Journal Fracture*, 93:115–144, 1998. [cited at p. 24]

[50] M Yoda. The j-integral fracture toughness for mode ii. *International Journal of Fracture*, 1980. [cited at p. 11]

Appendices

Appendix A

C++ code implementation for numerical simulations

A.1 Input and output files

In the following sections brief descriptions for the input parameters required by the code and the output results made by the code are presented. The units of the output results are the same as the units used for the input parameters. Note that the input and output files with `.msh` or `.pos` extensions can be viewed and edited by *Gmsh* software which is a 3D finite element grid generator with a build-in CAD engine and post-processor.

A.1.1 Input files

driverinfo.dat

In this file the main input parameters of a problem, most of them control parameters, are specified by the user. Note that the values of the control parameters are either 0 or 1 which means no and yes respectively. In the following a brief description of each parameter is provided.
`debug`: This control parameter is used to activate a version of the code that prints more outputs than usual about details of the problem. This version is used for code debugging purposes.
`thermocoupling`: This control parameter is used for the cases that the mechanical problem involves thermocoupling (not in the present study).
`compute_displacement`: This control parameter is used for the mechanical problems and is used to ask for the displacement field as an output file.
`compute_temperature`: This control parameter is used for thermal or thermo-mechanical problems and is used to ask for the temperature field as an output

file.
`degree`: This parameter is the degree of the polynomial shape functions used in the discretization with FEM.
`compute_sifs`: This control parameter is used to ask the code to compute the stress intensity factors and to print the results in an output file. Note that for cohesive crack model using the SIF-I criterion the value of this parameter should be 1.
`compute_stress_strain_work`: This control parameter is used to ask the code to compute the elastic stress-strain input energy of the system provided by the loads and to print the results in an output file.
`compute_error`: This control parameter is used to ask the code to compute the error of the FEM approximation. This parameter is used for the problems for which an analytical solution is available.
`solver`: In this parameter the name of the solver used for solving the system of equation of the problem should be provided. Note that different solvers should be provided and introduced to the code first. Note also that the numerical results obtained in the present study are obtained using *SuperLU* solver (see section 6.1).
`critical_k`: This parameter is the fracture toughness of the material.
`tensile_ultimate_strength`: This parameter is the ultimate tensile strength of the material (f_u).
`spring_k`: This parameter is the absolute value of the slope of the linear constitutive law used in the cohesive zone (see figure 2.6b). Note that for LEFM problems the value of this parameter should be 0.
`cohesive_distance_first_length`: This parameter is the first guess for the length of the cohesive zone of the first real crack length in the problem.
`crack_first_length`, `crack_step`, `max_length`: These parameters are the first length, the step and the maximum size of real crack required for the loop on real crack length.
`table_point_no`: The output data provided by the code are for the unset of each real crack propagation which means for each real crack length with its longest cohesive zone. But in order to obtain the data for a real crack with a cohesive zone smaller than the maximum cohesive zone (the data before unset of real crack propagation), some computations are done for a real crack with cohesive zone sizes smaller than the maximum size without performing any loop over length of cohesive zone. Note that the maximum size is known from previous computations from the loop over cohesive zone. The smaller cohesive zone sizes are obtained from the following formula:

$$L = \frac{i}{n} L_{coh} \quad i = 1, 2, \ldots, n \tag{A.1}$$

where L_{coh} is the maximum size and n is a value provided by `table_point_no` parameter.
`table_length_1`, `table_length_2`, `table_length_3`: The computations for obtaining the data before unset of real crack propagation is automatically performed for the first crack length (`crack_first_length`) (see section 6.4). In order to perform such computations for some other specific real crack lengths, these crack length should be provided in `table_length_1`, `table_length_2` and `table_length_3` parameters by the user. If such data are not required, the value -1 should be input for each parameter.
`max_no_itter`, `max_no_itter_load`: These parameters are the maximum number of iterations over 1-D segments and load factor respectively.
`mvfiles_address`: This parameter is the address of a script with the name `mvfiles.sh`. This script is used to put the post processing files for each crack length in a separate folder.
`results_dir_name`: In this parameter the main name of the folders in which the post processing files for each crack length will be moved is specified.
`output_disp_direction`: In this parameter the global direction of displacement (1, 2 or 3 for x, y and z respectively) to be extracted in post processing phase at some specific point in the problem is specified.
`output_disp_point`: In this parameter the point for which the displacement will be extracted in post processing phase is specified. Normally this point is the point of load application (as is in the present study).
`stress_eval_point`: In this parameter the point for which the stress values will be extracted in post processing phase is specified. This parameter is used for ultimate strength model and normally is crack initiation point (as is in the present study).
`lengthscale_W`: This parameter is the value of the length scale needed for computation of brittleness number (s_E). This value is used in post processing. In the present study it is the hight of the beam.
`Thickness_t`: This parameter is the value of thickness for 2D problems.
`no_crack`: This control parameter is used to ask the code not to include any cracks in the problem. It is used for ultimate strength models for beams without any initial cracks.

planercrack2d.dat

In this file more specific input parameters of the problem for each crack are specified by user. The parameters of each crack are in an special space starting with the name of the type of crack. For instance for a linear planer crack it is like the following:
`semiinfiniteplanecrack {...parameters ...}`

Note that crack types are defined in Xcrack library. In the following a brief description of each parameter of a linear planar crack is provided.
`crackname`: This parameter is the crack name which will be used to identify the output files associated to each crack.
`normaltotheplane`: This parameter is the vector which is normal to the crack plane.
`normaltothelip`: This parameter is the vector which is normal to the crack front.
`crack_init_point`: This parameter is the crack initiation point.
`enrichmenttype`: This parameter is the type of crack tip enrichment functions. The value should be `scalar_enrichment` or `vector_enrichment` for LEFM model and `cohesive_enrichment` for cohesive crack model.
`enrichmentradius`: The crack tip enrichment functions can be applied on the mesh nodes included in a domain around crack tip (see section 3.3.2). In Xfem library this domain is a circle and `enrichmentradius` parameter is the value of the radius of this circle.
`sifs_rho_geo`, `sifs_nb_layers_core`: In order to compute J-integral and interaction integral, the integration should be done over a domain around crack tip. In Xcrack library this domain is a circle and `sifs_rho_geo` is the radius of this circle. `sifs_nb_layers_core` parameter is number of layers of mesh element inside the empty domain around crack tip. Note that for cohesive crack model the value of `sifs_nb_layers_core` parameter can be 0.
`min_cohesive_distance`: This parameter is the minimum length of cohesive zone. This parameter is defined to avoid cohesive crack propagation problem to converge to complete LEFM (process zone with no length), which is the trivial solution of the problem (with load factor = 0).
`division_length_criteria`: This parameter is the maximum length of 1-D segments.
`crack_surf_division_number`: 1-D segments are created from crack surface mesh by dividing each crack surface segment, which is a line for 2D problems, by this number to equal portions (see `SplitSurfMesh` function in section A.2.3).
`fu_criteria`, `kI_criteria`: These control parameters are used to ask the code to use SIF-I or stress criterion respectively for real crack propagation in cohesive crack model.
`one_by_one`: This control parameter is used to ask the code to add or remove 1-D segments one by one in each iteration in the loop on cohesive length (as is the case for the results obtained in the present study).
`add_segments`: This control parameter enables the code to add 1-D segments to cohesive zone in addition to removing them during the loop on cohesive zone. This ability is used in algorithm 2 (see section 5.3.5).
`kI_tol`: This parameter is the value of the tolerance of the residual acceptable

for crack propagation criterion to be fulfilled.
`lf_first`, `lf_second`: These parameters are the values of first and second tries, used for linear extrapolation of critical load factor in algorithms 1 and 2 (see section 5.3.5) respectively.

Mesh file

The mesh file of the problem can be provided by any meshing software that is compatible with the code. For the present study *Gmsh* is used as meshing software.

material.dat

In this file the mechanical properties of the structure material are specified.

main2D.dat

In this file, which is the main input file, the type and the name of the mesh file as well as the names and the location of other input files should be provided by user. Dirichlet and Neumann boundary conditions for 2D problems are also prescribed in this file.

A.1.2 Output files

Output results for each real crack length

The files containing the computational results for each real crack length are put in separate folders. The name of these files with a brief explanation for each of them are presented below.
`Wcrt_itt_table.txt`: This file contains a table of the computational results for each iteration during the loop on the cohesive zone length for a problem with a specific real crack length. In this table the iteration number, the number of 1-D segments in the cohesive zone, the length of the cohesive zone, the crack opening at physical crack tip, the critical load factor, residual and the number of iterations performed to obtain the critical load factor (always 3 for algorithms 1 and 2) are presented in `Itter No.`, `1D-Seg No.`, `Coh_length`, `Last Seg Opn`, `Load F.`, `Residual` and `No.itter L.F.` respectively.
`crack name_crack front part.txt`: If in input files it is asked from the code to print the values of stress intensity factors, such values are printed in this file.
`load_def_for_len_itt_table`: This file contains the computational results for the first real crack length and for the crack lengths specified in the input files, with different cohesive zone lengths (see `table_point_no` input parameter in section A.1.1). For detailed explanation of each item in this file see section 6.2.2.
`crack name_crack part name_domain_for_integral.msh`, `frontmesh.msh`,

`1Dsegs.msh`: These files contain the mesh used for the computation of J-integral, the crack front mesh and the 1-D segments mesh used for the cohesive zone respectively.
`DISPLACEMENT.pos`, `STRESS.pos`, `lsn-name of crack.pos`, `lst-name of crack.pos`, `CRACK_OPENING.pos`: In these files the displacement field, the stress field, the crack normal and tangential level set fields and the crack opening filed for the whole crack are saved respectively.

Output results for the whole problem

General results of the whole problem for all real crack lengths are saved in a table as a text file with the name `results_table.txt`. Figure 6.4 shows an example of this table. See section 6.2.2 for the detailed explanation of each part of this table.

A.2 Main files of the code

There are some files that most of the procedures for the numerical solution are performed in them. In these files different classes are defined and also the facilities provided by other classes and libraries are used to set up the problem and solve it. These files and the new classes and functions defined in them for the present study are presented in this section.

A.2.1 main

In this files (`main.cc` and `main.h`) the general parts of the code are implemented. In this file the geometrical and mechanical parameters of the problem like the geometry of the structure, the location of the crack and the material properties, etc as well as the control variables are set from the input files. Using these parameters and variables the problem to be solved is established and the model to solve the problem (LEFM, cohesive crack model or ultimate strength) is determined. Note that many parts of the code are common for different models and the code will automatically skip the parts that are specific for each model using the control variables.

In `main.cc` a loop is defined on the real crack length so that the loading procedure is controlled by the real crack length. Inside this loop another loop is defined over the 1-D segments to determine the length of cohesive zone for each real crack length. For the first iteration the length of the cohesive zone is a user defined guess. During each iteration of the loop over the 1-D segments the following are performed:

- The crack is created using `xcCrack` class (see section A.2.3). Note that the mathematical crack tip will be determined from the sum of the length of the real crack and the length of the cohesive zone.
- The parameters of `Mechanics_c` class (see section A.2.2) are set.
- The system of equation is set up and solved using the `Mechanics_c` class. Note that the iteration on the load factor is done in this class.
- The results are extracted from `Mechanics_c` class and are printed in the output files and tables.

During each iteration over the 1-D segments the location of the crack and the whole system of equation is changed and again set up. When the iteration over the 1-D segments is converged the computations of the problem for one real crack length are finished and the results are obtained. The length of the cohesive zone obtained for a real crack length will be used as an initial guess for the length of the cohesive zone in the next iteration.

There are some overloaded functions defined in `main.h` to set the results in the output tables. According to the type of the problem and the model used an specific function will be used automatically to make the table. Note also that the results for each crack length are copied by the code automatically in separate folders in order to make the results more organized.

A.2.2 Mechanics

In these files (`Mechanics.cc` and `Mechanics.h`) the `Mechanics_c` class including the procedures for assembling the stiffness matrix of the problem, the inclusion of the enrichment functions and the solution of the system of equations are implemented. Some other classes and functions are also defined to make it possible to extract specific data from the results. Some general explanation of these classes are presented below.

`XevalFieldAtPoint`: This class takes a point (the mathematical crack tip in the present study) and evaluates the value of a field (the principal stress in the present study) at that point. This class is used as the main option in the code to evaluate the principal stress value at the mathematical crack tip in the case of using the stress criterion for the problem.

`XevalFieldMeanForPoint`: This class takes a point (the mathematical crack tip in the present study) and evaluates the mean value of a field (the principal stress in the present study) over the mesh element in which the point is located. This class is used as an option in the code to evaluate the mean value of the principal stress at the mathematical crack tip in the case of using the stress criterion for the problem.

`XacceptCrackSurfElement`: This class makes a filter on the 1-D segments. It

first sets the Gauss points for a desired degree for each 1-D segment (degree 7 to have four gauss points in the present study) and then evaluates the normal crack opening for each Gauss point. It returns false if for all of the Gauss points of a 1-D segment the normal crack opening is either bigger than the critical value or less than zero (with some tolerance).
`Mechanics_c`: This class is the most important class in the code. It uses the abilities provided by other classes and libraries to assemble the stiffness matrix of the problem, include enrichment functions and solve the system of equations. Below, a short general description of the new member variables and member functions of this class added or changed to include the cohesive crack model are presented.

Member variables

`spring_k`: This variable contains the value of the k parameter (the absolute value of the slope of the constitutive law in the process region, see figure 2.6b) provided by the input files.
`f_ult`: This variable contains the value of the ultimate tensile strength of the material provided by the input files.
`criticalopening`: This variable contains the value of the critical opening in the cohesive crack model provided by the input files.
`normall`: This variable contains the normal vector to the crack surface.
`kI_tol`: This variable contains the value of the tolerance of the residual acceptable for the real crack propagation criterion to be fulfilled. This value is provided by the input files.
`lf_first`, `lf_second`: These variables contain the values of the first and the second tries, used for the linear extrapolation of the critical load factor in algorithms 1 and 2 (see section 5.3.5) respectively. These values are provided by the input files.
`coh_dis`: This variable contains the length of the cohesive zone for a specific real crack length.
`coh_min`: In order to avoid the problem to converge to LEFM (real crack with no cohesive zone), which is the trivial solution of the problem (with load factor = 0), a minimum length is considered for the cohesive zone. This value is provided by the input files and saved in this variable.
`kI_I`: This variable contains the residual for each iteration during the loop on the load factor (see figure 6.4).
`opening_last`: This variable contains the normal crack opening for the last 1-D segment away from the mathematical crack tip of the crack.
`max_no_itter_load`: This variable contains the maximum number of iterations for the loop over the load factors provided by the input files.
`add_segments`: This is a control variable. If the value of this variable is one,

the code is able to add 1-D segments to the cohesive zone during the loop over the 1-D segments (to increase the length of the cohesive zone). In other cases it should be 0. Note that the value of this variable should be 1 for algorithm 2.
`fu_criteria`, `kI _criteria`: These control variables are used in order to select between different criterion for the real crack propagation. If `fu_criteria` is 1, the stress criterion will be used and if `kI_criteria` is 1, the SIF-I criterion will be used for the problem.
`oneDsegments_Vect`: This variable is a vector variable that contains the whole 1-D segments created from the crack surface mesh and sorted (see section A.2.3).
`oneDsegments_Coh`: This variable is a vector variable that contains the 1-D segments that are included in the cohesive zone. Note that the cohesive zone is identified by the `coh_dis` variable.

Member functions

`compute_sifs`: This function computes the stress intensity factors and prints them in an output file. It also returns the value of k_I. This function is used in algorithms with SIF-I criterion.
`AddRemoveSegments`: This function adds or removes the 1D segments from the cohesive zone (`oneDsegments_Coh` variable) according to `XacceptCrackSurfElement` filter. It also returns the 1-D segment that is added or removed from the cohesive zone.
`computeExternalForcesWork`: This function computes the elastic stress-strain energy input in the system provided by the load until the real crack propagation.
`formulationMechanics`: This function first assembles the stiffness matrix of the problem for a mechanical problem and includes the enrichment functions. Then it sets up the system of equations. Next it makes a loop on the load factor and finds the critical load factor using either of the stress or SIF-I criteria for a crack with a constant cohesive length. Then using `AddRemoveSegments` function it checks if it is needed to add or remove 1-D segments from cohesive zone. Finally it saves the critical load factor for a specific cohesive length and also the next mathematical crack tip (note that as explained in section 5.3.5 in algorithm 2 the 1-D segments are added or removed from the last segments away from the physical crack tip).
`addCrack`: This function adds the crack made by `xcCrack` class (see section A.2.3) to the crack list of `Mechanics_c` class and at the same time it reads the input data provided by `planercrack2d.dat` input file.
`applyDirichletToMechanics`: This function applies the mechanical essential (Dirichlet) boundary conditions to the problem according to `main2D.dat` input file.
`applyNeumannToMechanics`: This function applies the mechanical Neumann

boundary conditions to the problem. This function is overloaded. One version just applies the forces whose values and locations are provided by `main2D.dat` input file. This version is used for LEFM and ultimate strength models. The other version multiples the forces provided by `main2D.dat`, by the load factor whose value is obtained in the loop over the load factor. This version is used for cohesive crack model.
`applySpringsBilinearOnCrack` : This function assembles the integration on the cohesive zone on l.h.s of (5.8) to the stiffness matrix.
`applySpringsLinearOnCrack`: This function assembles the integration on the cohesive zone on r.h.s of (5.8) to the load vector in the system of equations.

A.2.3 xcCrack

In these files (`xcCrack.cc` and `xcCrack.h`) some functions and class hierarchies are defined to build the cracks defined in the input files using level set techniques, to add the crack tip enrichment functions to the stiffness matrix and also to create the 1-D segments mesh from the crack surface mesh. Some general explanation of these classes and functions are presented below.
`buildcrackfromstream`: This function uses the proper functions and classes to build a crack from the input data provided by `planercrack2d.dat` input file. It takes the mesh of the problem, the access to the input file, the real and cohesive crack lengths and the mathematical crack tip as arguments.
`xcCrack`: This class is the base of a class hierarchy and provides the general tools to build a crack as well as some functions that are overloaded in the derivative classes. Note that each object of this class represents a crack and contains the whole information and data for that crack in its member variables.
`xcCrackPlanarLine`: This class is derived from `xcCrack` class and overloads and provides the functions specific for linear planar cracks.

There are some other classes derived from `xcCrack` class that are defined for special crack shapes and geometries. These classes are: `xcCrackPlanarDisk`, `xcCrackCylinderLine` and `xcCrackLens`.

Below, a short general description for the new member variables and member functions of `xcCrack` class hierarchy added or changed to include cohesive crack model is presented.

Member variables

`crack_surf_split`: This variable is a `xMesh` variable (see section A.3.1) that contains the whole 1-D segments created from the crack surface mesh (see section A.2.3).
`crack_surf_sorted`: This variable is a vector variable that contains the whole 1-

D segments created from the crack surface mesh that are extracted from `crack_surf_split` variable and sorted (see section A.2.3).
`crack_surf_sorted_dist_org`: This variable is a vector variable that contains the sorted 1-D segments of `crack_surf_sorted` variable that are included in the cohesive zone.
`real_tip`: This variable contains the real (physical) crack tip point.

Member functions

`xcCrackPlanarLine`: This function is the constructor of `xcCrackPlanarLine` derivative class. This function reads the crack data from `planercrack2d.dat` input file. Then taking the real and cohesive crack lengths as arguments and using the crack initiation point and the normal vector to the crack lip provided by `planercrack2d.dat` input file (see section A.1.1) it identifies the real and fictitious crack tip points. Finally it builds the crack calling `setup` member function.
`setup`: This function creates the crack by means of `lCrack` class (see section A.4) and by establishing the two level sets required to represent the crack (see section 3.3.3).
`SplitSurfMesh`: This function creates the 1-D segments required for the integration over the cohesive zone from the crack surface mesh using a complicated algorithm. It takes the 1-D mesh of the crack surface and then it creates the 1-D segments by dividing this mesh. The division procedure is in a way that the 1-D segments start from and end to the physical and mathematical crack tips. The number of devisions as well as the maximum size of the 1-D segments are provided by `planercrack2d.dat` input file. The 1-D segments created are saved in `crack_surf_split` member variable.
`SortCrackSplitSurfaceMesh_ExtractCoh`: This function extracts the 1-D segments from `crack_surf_split` member variable. Then it sorts them according to their distance from the mathematical crack tip and saves them in `crack_surf_sorted` member variable. It also extracts the 1-D segments sorted that are in the cohesive zone (using the cohesive length) and saves them in `crack_surf_sorted_dist_org` member variable.

A.3 Xfem library

A.3.1 Basic classes

In this section some basic and important classes used in Xfem library are explained in brief.
`xApproxFunction`: This class is the basic class of a class hierarchy that makes it possible to define the shape functions. Some member functions are also defined to evaluate the value of the shape functions, their gradient and Hessian at any

point.
`xAssembler`: This class is the basic class of a class hierarchy that makes it possible to assemble the finite element vectors, matrices and scalars.
`xData`: This class generally organizes the process of reading and saving the input data from the input files.
`xField`: This class provides the tools to make a filed from a value space and a mesh. It also provides the tools to evaluate the field and its gradient.
`xLevelSet`: This class provides the tools to define a level set on a mesh and to evaluate the value of the level set and its gradient at any point.
`xEval`: This class is the basic class of a class hierarchy that makes it possible to evaluate the value of different functions (like stress, strain, crack opening, etc) with different natures (unary, binary, constant, etc) at a point using the displacement filed obtained from the solution of the system of equation.
`xMesh`: This class is derived from `mMesh` class of the *AOMD* package. It adds the functionality to create a subset of a mesh. A subset is a group of mesh entities for which a name is associated. `xMesh` offers the possibility to iterate on a subset.

AOMD (Algorithm Oriented Mesh Database) is a mesh management library (or database) that is able to provide a variety of services for mesh users. The optimal form of the mesh representation is application dependent with different applications requiring different sets of mesh adjacencies.

Xfem library contains many of other important classes that are not mentioned here for being brief.

A.3.2 New classes and functions

In the following the new classes and functions implemented by the author of the present thesis in Xfem library specifically for cohesive crack model are presented in brief.
`xEvalFieldOnCrack`: This class is derived from `xEval` class and is defined to make an interface for evaluation of the crack opening. This class is defined in `xField.h` file.
`GetValOnCrack`: This is a member function of `xField` class which evaluates the normal displacement on different sides of the crack surface and finally evaluates the crack opening. Changing of crack surface side is possible by changing the value of a variable called `normalOriented_tag` to either 1 or -1.

A.4 Xcrack library

A.4.1 Basic files and classes

In this section some basic and important files and classes used in Xcrack library are explained in brief.

`FunctionCrackXFEM`: In these files (`FunctionCrackXFEM.h` and `FunctionCrack-XFEM.cc`) some classes are defined to define and evaluate the discontinuous and crack tip enrichment functions. These classes are generally derived from `xEal` and `xApproxFunction` classes from Xfem library.
`lCrack`: This class creates a crack from two level sets (see section 3.3.3). It also provides the tools to create the crack surface and the crack front meshes as well as the tools to identify the side of the crack, the elements cut by the crack, the elements containing the crack tip, etc.
`xcFormLinearEnergyRelease`: In these files (`xcFormLinearEnergyRelease.h` and `xcFormLinearEnergyRelease.cc`) some classes are defined to compute J-Integral and energy release rate for a crack.
`xcInteractionIntegralsOnCrack`: In these files (`xcInteractionIntegrals-OnCrack.h` and `xcInteractionIntegralsOnCrack.cc`) some classes are defined to compute the interaction integral and the stress intensity factors. In these files `crackFrontPart` class is the base class of a class hierarchy that makes it possible to define a part of the crack front, simply connected or a loop. There is another class named `xcInteractionIntegralsOnCrack` that provides the tools to compute the interaction integral and the stress intensity factors along such crack part.

A.4.2 New classes and functions

In the following the new classes and functions implemented in Xcrack library which are specific for cohesive crack model are presented in brief.
`ScalarFunctionCrackTipCohesive1_c`: As explained in section 5.3.3 for cohesive crack model, nonsingular branch functions are needed to enrich the field around the crack tip. This class is defined to make an interface to evaluate the value of the function $r\sin(\frac{\theta}{2})$, used in the present study, and its gradient at different points of the domain. This class is defined in `FunctionCrackXFEM` files.

Since in cohesive crack model the crack surfaces are not traction free the terms in J-integral that are integrated over the crack surfaces should be taken into account. For this aim some modifications are done in the files related like `xcInteractionIntegralsOnCrack`, `xcFormLinearEnergyRel- ease`, etc. Such modifications are not explained here for being brief.

List of Figures

2.1 Different loading modes 8
2.2 Notations for J-integral 11
2.3 Strain softening in different materials 12
2.4 Bažant's size effect law 14
2.5 Process zone in cohesive crack model (figure from [17]) 16
2.6 Constitutive law inside and outside process region 17

5.1 Domain and notations for specimen with cohesive crack 28
5.2 A zoom in cohesive zone 28
5.3 Algorithm 1 for cohesive crack propagation 32
5.4 Algorithm 2 for cohesive crack propagation 33

6.1 Geometry and boundary conditions of the three point bending test . . 36
6.2 Undeformed mesh and deformed shape of the beam with a crack . . . 37
6.3 Non-dimensional load-deflection curves for three point bending test . . 38
6.4 Output table for three point bending test with $G_f = 50\,Nm^{-1}(s_E = 1e^{-4})$ 39
6.5 Mesh for the domain and cohesive zone 41
6.6 Non-dimensional load-deflection curves for different values of Nc and a constant mesh size (m = 17) with the length of 1-D segments not divided 42
6.7 Non-dimensional load-deflection curves for a material with constant brittleness number ($s_E = 2e^{-5}$) and different mesh sizes and with the length of 1-D segments not divided 43
6.8 Non-dimensional load-deflection curves for constant brittleness number $s_E = 2e^{-5}$ and constant mesh size (m = 8) but with different sizes of 1-D segments 44
6.9 Non-dimensional load-deflection curves for different values of Nc and a constant mesh size (m = 17) with the length of 1-D segments divided by three 44

6.10 Non-dimensional load-deflection curves for a material with constant brittleness number $s_E = 2e^{-5}$ and different mesh sizes and with length of 1-D segments divided by three 45
6.11 Non-dimensional load-deflection curves for brittleness number $s_E = 2e^{-5}$ and different mesh sizes and with length of 1-D segments divided by three (Stress criterion vs SIF-I criterion) 47
6.12 Non-dimensional load-deflection curves for different values of brittleness number for a beam with no initial crack 48
6.13 Non-dimensional load-deflection curves for different sizes of the beam for a beam with no initial crack 48
6.14 Load-CMOD curves for different values of brittleness number for a beam with no initial crack 49
6.15 Length of cohesive zone as a function of inverse of brittleness number for three point bending test with $a_0/h = 0$ 50
6.16 Non-dimensional load-deflection curves using LEFM model for different values of brittleness number for a beam with no initial crack . . . 50
6.17 Non-dimensional load-deflection curves for different values of brittleness number for a beam with an initial crack depth of $a_0/h = 0.1$ . . . 51
6.18 Non-dimensional load-deflection curves for different values of brittleness number for a beam with an initial crack depth of $a_0/h = 0.3$ . . . 52
6.19 Non-dimensional load-deflection curves for different values of brittleness number for a beam with an initial crack depth of $a_0/h = 0.5$ . . . 52
6.20 Non-dimensional load-deflection curves for $s_E = 1e^{-4}$ for a beam with different initial crack length 53
6.21 Non-dimensional load-deflection curves for $s_E = 2e^{-5}$ for a beam with different initial crack length 54
6.22 Length of cohesive zone as a function of inverse of brittleness number for three point bending test for a beam with different initial crack lengths 54
6.23 Apparent strength v.s. real strength of the material for different values of brittleness number for a beam with no initial crack 55
6.24 Elastic and elastic perfectly plastic distribution of stress in the center of the beam 56
6.25 Fictitious fracture toughness v.s. real fracture toughness of the material for different values of brittleness number for a beam with an initial crack depth of $a_0/h = 0.5$ 57